Order Number 1355180

A quasi-elastic neutron scattering study of hydrogen dynamics in trypsin-D_2O solution

Cao, Hung Duc, M.A.

Rice University, 1993

U·M·I
300 N. Zeeb Rd.
Ann Arbor, MI 48106

RICE UNIVERSITY

A Quasi-elastic Neutron Scattering Study of Hydrogen Dynamics in Trypsin-D_2O Solution

by

HUNG CAO

A THESIS SUBMITTED
IN PARTIAL FULFILLMENT OF THE
REQUIREMENTS FOR THE DEGREE

MASTER OF ARTS

APPROVED,THESIS COMMITTEE:

Harold E. Rorschach

Harold E. Rorschach, Jr., Chairman
Professor of Physics

Carlton F. Hazlewood
Adjunct Professor of Biophysics

George T. Trammell
Professor of Physics

Gordon S. Mutchler
Professor of Physics

Houston, Texas
January, 1993

Abstract

A Quasi-Elastic Neutron Scattering Study of Hydrogen Dynamics in Trypsin-D_2O Solution

by

Hung Cao

The quasi-elastic neutron scattering (QNS) method is a useful technique to study biomolecular dynamics. The versatility of the method makes possible motional studies of biomolecules in different forms: powder, crystalline, and solution; and at different temperatures. Thus, it allows investigation of biomolecular dynamics in different states of matter. We have used the QNS method to study the motion of the trypsin chain segments in powder and in D_2O solution at temperatures of 200K, 280K, and 300K. The scattering spectra $S(Q,\omega)$ were measured in constant-Q mode. The $S(Q,\omega)$ for trypsin protons in liquid solution exhibits a broadening due to diffusive motion which is absent in the powder and the frozen solution. This diffusive motion has the character of a jump diffusion. The high-frequency thermal motion obtained from the Debye-Waller factor $\langle u^2 \rangle/3 \cong 0.33 Å^2$ at T=300K is consistent with earlier measurements. The DW factor at lower temperatures for trypsin solution shows deviation from theoretical predictions.

Acknowledgements.

Dr. H. E. Rorschach and Dr. C. F. Hazlewood have allowed me to work with them in the pursuit of nature secrets in this fascinating field. Their enthusiasm and sense of humor are infectious.

I would like to express my gratitude and respect to Dr. H. E. Rorschach for his guidance, patience, support and great physical insights. Without him, I would still be working on this thesis.

I also would like to express my appreciation and respect to Dr. C. F. Hazlewood for his encouragement, support in every phase of my thesis.

People at Brookhaven National Laboratory were very supportive and helpful. I would like to thank Dr. S. Shapiro and Dr. T. Thurston for their help and useful discussions. They made the experiment possible and enjoyable.

Dr. G. N. Phillips and his students are appreciated for their great help in successful crystal growing and preparing biological samples.

Our pilot experiment were possible due to the assistance of Dr. R. Nicklow at Oak Ridge National Laboratory. His help is appreciated.

I would like to thank Dr. G. T. Trammel for his willingness to serve on the thesis committee, his discussion is always appreciated. I would like also to thank Dr. G. S. Mutchler for his help in improving my thesis.

My fellow graduate students Eric Smith, Chen Lin, and Kevin Minard will always be remembered for their support and enlightening discussions.

I am very thankful to have a wonderful family.

This work was funded by the Department of Energy and the R. A. Welch Foundation.

TABLE OF CONTENTS

List of Figures.

I. Introduction.

A. *Importance of Biomolecules.*

The functional roles of biomolecules are essential to life. They are responsible for maintaining cells, organs; carrying genetic codes; conducting nerve signals; catalyzing biochemical reactions; transporting and storing charge and matter; and all other bio-processes[1]. A class of biomolecules, called proteins, are made up of amino acids, the 20 building blocks of life. These biomolecules often fold into complex three-dimensional structures. These structures exist in many configurations, or states, of nearly equal energy – often called microconformations, or conformational substates – separated by energy barriers. These substates are the result of small shifts in position of various segments of the molecules[2].

Due to their important but complex nature, biomolecules have attracted much attention in recent years. Their characteristics make them ideal candidates for exploring the physics of complexity, a recent trend in science. So what physics can we learn from these biomolecules? As Fraunfelder summarized, we can take clues from well-established fields of physics like atomic, condensed-matter, or particles physics. Experimental discoveries in these fields often come from studies of structure, energy levels, and dynamics[2]. It is the dynamical aspect that we want to discuss here, but it is also necessary to understand the structure and energy levels of the biomolecule.

B. *Techniques for Probing Protein Motions.*

The complexity of biomolecules requires more than one technique to fully explore their nature. Several techniques have been used: light scattering, X-ray and neutron diffraction, small-angle neutron scattering, nuclear magnetic resonance (NMR), Mössbauer spectroscopy, flash photolysis, inelastic neutron scattering, computer simulation, quasi-

elastic neutron scattering (QNS), etc.[2] . We have used the QNS method to investigate the motion of biomolecules. In this thesis, we discuss computer simulation, as well as QNS, since some of its related results are compared with our experiment.

C. *Computer Simulation Techniques.*

Computer simulation has provided insights in bridging the gap between theory and experimental properties of the dynamical biomolecules. Several techniques used in computer simulations include molecular dynamics (MD), stochastic dynamics (SD), energy minimization (EM), normal mode (NM), and Monte-carlo (MC) simulation[3,4,5,6].

The basic principle of MD is the employment of numerical integration methods to trace the Newtonian equations of motion of interacting particles over a certain length of time, usually on the order of a few hundred picoseconds. The simulation may place the biomolecule in an aqueous environment, water in most cases. The atoms are assigned initial coordinates, determined from X-ray diffraction, and initial velocities, chosen from a Maxwellian distribution for a given temperature. The force acting on a particular atom is obtained from taking the derivative of the potential energy (PE) function with respect to its position. The PE consists of many terms. Theoretically, these could be determined from the Schrodinger equation. In reality, only a few simple models can be treated in this way. Instead, the PE function is determined empirically. It contains terms for covalent-bond stretching, bond-angle bending, harmonic dihedral bending, sinusoidal dihedral torsions and non-bond (van der Waals and Coulombic) interactions. Quantum correction to this approach have been shown to be small and only significant for local vibrations at frequencies greater than 300 cm^{-1}.

SD is an extension of MD. The particles' motion is followed by numerical integration of the stochastic Langevin equations of motion.

The EM approach searches for equilibrium configurations by numerically moving toward the minimum of the PE function.

NM analysis assumes that the system undergoes harmonic motion about its equilibrium position, which is the minimum energy configuration. In this sense, it relates to the EM approach.

MC simulation uses a random-walk technique on the PE surface, sampling many configurations using the Boltzmann factor as the weight function.

One assumption of the NM and EM method is questionable, namely that the biomolecule executes harmonic motion about its equilibrium position. Indeed, there is much evidence against this hypothesis. MC's results give static properties. That leaves SD and MD as two promising methods which yield both static and dynamic properties, and possible anharmonic behaviors. The results mention in this thesis are from MD.

At the present stage, computer simulations can handle crystalline and gas systems easily, using both classical and quantum treatments. It is still impossible to simulate the biomolecule in solution quantum-mechanically. Classically, the simulation must be done by brute force. What is often done is to reduce the problem to fewer degrees of freedom, or fewer particles (so it is like the crystalline state) by symmetry or by dilution respectively[3]. So in the comparison of the simulation results and experimental data, all these limitations must be taken into consideration.

Much work has been done on MD simulation, but there are few experimental data on the basic motion at the picosecond time-scale to compare with the simulations, which would give a verification of the existence of picosecond fluctuations. QNS mainly extends to the region of energy transfer $\omega \approx 0$ ($\pm$ 2meV), which samples the diffusional or rotational motion of the biomolecules. The time scale is between 10^{-10} - 10^{-12} s[6]. The motion of the atoms produces a Doppler broadening of the elastic line. The scattering is

mainly due to hydrogen atoms, since the proton has such a large incoherent scattering cross section that the scattering by other elements can be neglected.

D. *The Main Work of This Thesis.*

The purpose of our work is to employ QNS methods to explore the dynamics of chain segments of biomolecules, in this case trypsin, which has been studied by computer simulations. Previous work related to ours will be discussed and compared with our results. Some relevant results from MD simulations will also be mentioned, especially the recent work by A. E. Garcia<7>.

E. *Previous Experimental Work .*

QNS studies of trypsin motion were done by D. Bearden and C. Lin<8,9>. Bearden studied the high frequency thermal vibrational motion of hydrogen in trypsin by measuring S(Q) – the integrated intensity of the quasi-elastic peak. From these data, the mean-squared local vibrational amplitude can be extracted from the Debye-Waller (DW) factor. However, the details of the atomic diffusive motion can not be obtained in this way because no information on the line shape is obtained. Corrections for background, spectrometer-resolution, and inelastic scattering proved to be very difficult using this low-resolution QNS technique.

C. Lin made high-resolution QNS measurements on "treated" trypsin powder (freeze-dried lyophilized trypsin powder) and 20% by weight "treated" trypsin in D_2O solution. This high-resolution technique was used to avoid the previously encountered problems in Bearden's experiment, and to obtain details on the diffusional motion of trypsin chain segments. One shortcoming was the large background due to the spectrometer

configuration, which caused large statistical errors in the point-by-point background subtraction technique.

Our experiments were similar to those of C. Lin. Both high and low resolution scans were taken on trypsin powder and 20% by weight trypsin in D_2O solution. We also plan to study trypsin in the crystalline state to compare the dynamics in the crystal and the solution.

II. Trypsin and Sample Preparation.

A. *Properties of Trypsin.*

Trypsin is an enzyme released from the pancreas. It is responsible for the hydrolysis of peptide bonds in proteins and peptides. Trypsin has many covalently bonded hydrogens on the surface which can exchange with solvent hydrogens. About 60% of the trypsin residues are classified as internal and inaccessible to solvent molecules. Trypsin consists of 223 amino acids and about 154 solvent molecules. The structure type of trypsin is mostly β form. There are, however, a few small sections that maintain α helical structure (from residues 164 to 168; 234 to 239; 241 to 244). The number of protein ligands hydrogen-bonded to water molecules is 101. Out of 101 hydrogen-bonded ligands there are 188 bonded sites. Trypsin has been shown to undergo three reversible pH-dependent conformation changes between pH 0.5 and pH 7.0, and is most active between pH 7.0 and 9.0. In an H/D exchange study of trypsin crystals (one year at pH 7 and 20^0C), Kossiakoff found that, out of 215 exchangable amide peptide groups in trypsin, 68% were found to be fully exchangable, 8% partially exchanged and 24% unexchanged<10,11,12,13>.

Trypsin has the ability to digest itself. Chymotrypsin, which has a structure similar to trypsin, is relatively invulnerable to autodigestion, since the bonds that it cleaves best are close to side chains which are generally located in the interior of the chymotrypsin molecule. Therefore, these bonds are restricted and can not move around to damage the molecule. Unlike chymotrypsin, trypsin cleaving-bonds are close to basic side chains which are always exposed on the outside of the molecule, and thus it is very susceptible to autodigestion – a process that often makes biochemical or crystallographic experiments with native trypsin difficult<10>.

In crystal form, the trypsin molecule folds up in two halves. Each has a pseudo-cylindrical arrangement of hydrogen bonds between adjacent anti-parallel extended chains

similar to that described by Blow for α-chymotrypsin. Any motional change in the interior of the molecule is often accompanied by a second one which is correlated with it and thus allows the main chain folding to remain stable<10>.

B. *Sample Preparation and Data Scans.*

Since our experiment is designed to look at the motion related to the trypsin itself, namely the hydrogens associated with the molecule, D_2O is used as the solvent. Initially, the loosely bound hydrogens were exchanged with deuterons by the following procedures. First, the raw trypsin powder was mixed with D_2O in a closed container at about 6% concentration. The sample was left in a refrigerator at about 3^0C for about 20 hours. Then we placed the sample in an ethyl alcohol + dry-ice bath to freeze-dry it. Next, the sample was placed in a vacuum chamber for about 30 hours to remove the solvent. The resulting trypsin is called "treated" trypsin.

In the experiment, the treated trypsin was mixed with D_2O to form a solution. The pH of the solvent was adjusted with DCl to fall in the range 4 - 5 to prevent the trypsin from self-digestion. The sample was placed in a cryostat filled with He gas during the neutron scattering experiment for temperature-control purposes and to prevent the condensation of water on the sample container surface. There are two different designs of the aluminum sample chambers. One is made for holding dry samples. The other is made for holding liquid samples to minimize the liquid loss during the experiment (see Fig. 1a&b).

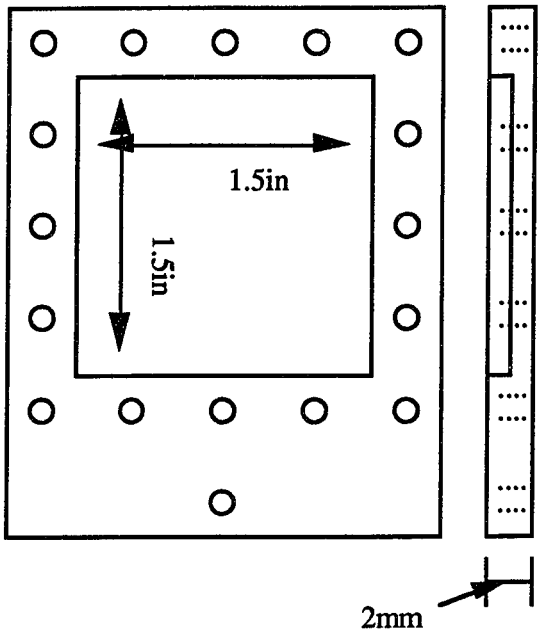

Fig. 1a. Al chamber for holding dry sample.

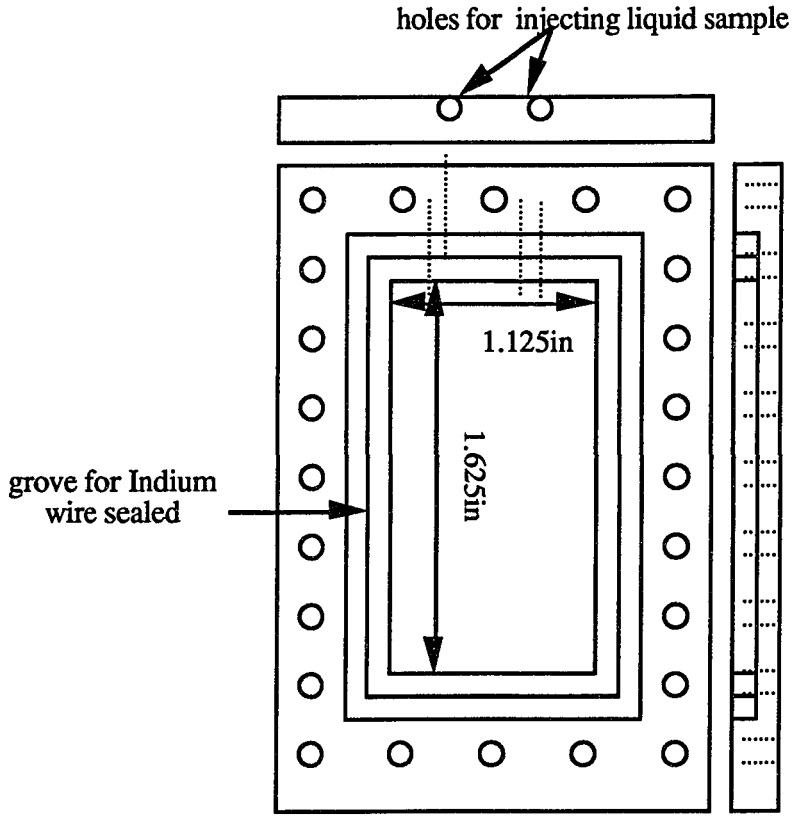

Fig. 1b. Al chamber for holding liquid sample.

III. Basic Properties of the Neutron.

The neutron has

mass:	1.675×10^{-27} kg
charge:	0
spin:	$\frac{1}{2}$

magnetic dipole moment : $\mu_n = -1.913\ \mu_N$.

The importance of thermal neutrons comes from the basic properties of the neutron as listed above. The energy of a neutron with velocity v is its kinetic energy $\frac{1}{2} mv^2$ with wave vector

$$\mathbf{k} = \frac{m}{\hbar} \mathbf{v} \tag{3-1}$$

and wavelength

$$\lambda = \frac{2\pi}{|k|} = \frac{h}{mv}. \tag{3-2}$$

Thermal neutrons emerging from reactor have a Maxwellian velocity spectrum. The flux distribution is then

$$\phi(v)\, dv \sim v^3 \exp\left(-\frac{1}{2}\frac{mv^2}{k_\beta T}\right) dv \tag{3-3}$$

where, T = temperature of the moderator

$\phi(v)\, dv$ = number of neutrons per unit area per second with velocities between v and v + dv

m = neutron mass

k_β = the Boltzmann constant.

The maximum of the function $\phi(v)$ occurs when $v = (\frac{3k_\beta T}{m})^{\frac{1}{2}}$ corresponding to a K. E. of

$$\text{K.E.} = \frac{1}{2}mv^2 = \frac{3}{2}k_\beta T. \tag{3-4}$$

Normally, the neutron energy E is described by a temperature T through the relation $E = k_\beta T$. The momentum of the neutron is $\mathbf{p} = \hbar\mathbf{k}$. And by convention, we have

$$\text{K.E.} = k_\beta T = \frac{1}{2}mv^2 = \frac{1}{2}\frac{h^2}{m\lambda^2} = \frac{1}{2}\frac{\hbar^2 k^2}{m}. \tag{3-5}$$

Substituting the values for m, e, ħ, k_β into (3-5) gives

$$\lambda = 6.283\frac{1}{k} = 3.956\frac{1}{v} = 9.045\frac{1}{\sqrt{E}} = 30.81\frac{1}{\sqrt{T}} \tag{3-6}$$

$$E = 0.086T = 5.227v^2 = 81.81\frac{1}{\lambda^2} = 2.072k^2, \tag{3-7}$$

where λ is in Å, k in 10^{-10} m^{-1}, v in $\frac{km}{s}$, E in meV, and T in Kelvin. Other units often used in neutron spectroscopy are

$$1meV \equiv 0.24THz \equiv 8.07cm^{-1} \equiv 11.61K.$$

Neutron beam often are classified as being cold (.1–10meV), thermal (5–100meV), hot (100–500meV), or epithermal (>500meV). In our experiment, we mainly used cold neutrons<14,15,16,17,18>.

As mentioned earlier, the neutron's basic properties make it an important tool for studying the static and dynamic properties of condensed matter. To study the static structure of macromolecules, the radiation needs to have a wavelength comparable in

magnitude with the spatial dimensions between atoms. To probe the dynamical properties of macromolecules, the radiation frequencies must be on the order of the vibrational frequencies of the atoms. X-ray and infra-red radiations meet the static and dynamic requirements respectively. Thermal neutrons satisfy both requirements.

Another reason for the importance of the neutron's properties is the interaction between the neutron and nuclei. The scattered amplitude of the neutron scattered by an atom depends on the nucleus' characteristics and so the amplitude varies between different isotopes of the nucleus and between different nuclei. For certain nuclides, the incoherent scattering amplitude, the absence of interference between waves scattered by different atoms, is large; e.g. hydrogen, which is almost invisible to X-rays, is a strong neutron-scatterer.

As a quantum object, neutrons are characterized by wave functions $|\mathbf{k}\rangle$ such that

$$|\mathbf{k}\rangle = \frac{1}{\sqrt{V}} \exp(i\mathbf{k}.\mathbf{r}) \qquad (3\text{-}8)$$

where V is the volume of quantization, (the same as the volume of the irradiated sample). The density of states of momentum **k** in this volume is given by[19]

$$\rho(\mathbf{k}) = \frac{V}{(2\pi)^3}. \qquad (3\text{-}9)$$

IV. Neutron Scattering.

A. *Neutron - Nucleus Interaction.*

A neutron and a nucleus interact via nuclear and magnetic forces. Since the nuclear force is short range compared to the thermal neutron wavelength, it can be shown that the interaction potential between a neutron positioned at $\mathbf{r}$ and a nuclei i at $\mathbf{r}_i$ can be written as

$$V(\mathbf{r}) = \frac{2\pi\hbar^2}{m_n} b_i \, \delta(\mathbf{r} - \mathbf{r}_i). \qquad (4\text{-}1)$$

This is often called the Fermi pseudo-potential<20,21>. The scattering length b_i is independent of the neutron energy and is a characteristic of the interaction. It can be negative or positive depending on the repulsive or attractive nature of the interaction. The determination of b_i is very difficult theoretically and is usually done experimentally. In the magnetic interaction, the neutron interacts with the spins by the dipole-dipole coupling. For diamagnetic systems, it is always negligible compared to the nuclear interaction and will not be considered.

B. *Coherent and Incoherent Scattering Lengths, and Cross Sections.*

In a system of a given atomic species i, with many isotopes having a nuclear spin, the b_i will change from one atom to another, since the interaction depends on the properties of the nucleus and on the total spin state of the nucleus-neutron system.

The coherent scattering length is the average $< b_i >$ of b_i over all the isotopes and spin states. The incoherent scattering length is the mean square deviation of b_i from $< b_i >$. We thus have

$$b_i^{\,coh} = < b_i > \qquad (4\text{-}2)$$

$$b_i^{\,incoh} = [\, < b_i^{\,2} > - < b_i >^2 \,]^{\frac{1}{2}} . \qquad (4\text{-}3)$$

It is clear that $b_i^{\,coh}$ and $b_i^{\,incoh}$ can be varied by changing the relative concentration of the various isotopes. This point has important applications in neutron experiments, thru the isotopic substitution technique. The coherent and incoherent scattering cross-section are defined as<20>

$$\sigma_i^{\,coh} = 4\pi\,(b_i^{\,coh})^2 \qquad (4\text{-}4)$$

$$\sigma_i^{\,incoh} = 4\pi\,(b_i^{\,incoh})^2 . \qquad (4\text{-}5)$$

C. *Neutron Scattering Functions.*<15,16,18,19,21,22>

An elegant quantum technique to derive the neutron scattering function by F. Volino is given in Appendix A. We however choose to derive it in a more conventional way. We define the neutron N, the sample S, and the interaction hamiltonian H_C. The neutrons are described by their plane wave functions $|\mathbf{k}>$. The sample is made up of M particles i located at $\mathbf{r}_i$. The coupling between S and N is given by the Fermi pseudo-potential, summed over all the particles i,

$$H_C = \frac{2\pi\hbar^2}{m_n} \sum_i b_i\, \delta(\,\mathbf{r} - \mathbf{r}_i\,). \qquad (4\text{-}6)$$

The neutrons are generally well collimated and monochromatized, so they are in a well defined state $|\mathbf{k}_0>$. The interest is in the probability of the neutrons to make a transition to another state $|\mathbf{k}_1>$. The amplitude of this transition $\overline{H_C}$ can be written as

$$<\mathbf{k}_1|\ H_C\ |\mathbf{k}_0> = \frac{1}{V}\,(\frac{2\pi\hbar^2}{m_n{}^2}) \sum_i b_i \exp\,(\,i\mathbf{Q}.\mathbf{r}_i\,) \qquad (4\text{-}7)$$

where $\mathbf{Q} = \mathbf{k}_0 - \mathbf{k}_1$, is the neutron momentum transfer. In experiments, a beam of monochromatic neutron $\mathbf{k}_0$ is scattered from a sample, and detectors collect the scattered neutrons with momenta between $\mathbf{k}_1$ and $\mathbf{k}_1 + d\mathbf{k}_1$. Let the number of incident neutrons per cm^2 per sec be I_0 . The sample has the volume V (a cylinder with cross section S and length l). The number of incident neutrons on the sample is $I_0 (\frac{V}{v_0})$ where v_0 is the incident velocity. Let I be the number of neutrons scattered per second between $\mathbf{k}_1$ and $\mathbf{k}_1 + d\mathbf{k}_1$, $W_{\mathbf{k}_1 \mathbf{k}_0}$ be the probability per unit time that gives the change of the state of the neutron, (see App. A) then

$$I = I_0 (\frac{V}{v_0}) \; W_{\mathbf{k}_1 \mathbf{k}_0} \; \rho(\mathbf{k}_1) \; d\mathbf{k}_1 . \tag{4-8}$$

$$\rho(\mathbf{k})d\mathbf{k} = \frac{V}{2\pi^3} \tag{4-9}$$

$$\frac{I}{I_0} = \frac{V}{v_0} \; W_{\mathbf{k}_1 \mathbf{k}_0} \; \rho(\mathbf{k}_1) \; d\mathbf{k}_1$$

$$= \frac{\hbar}{m_n} \frac{k_1}{k_0} \sum_{ij} \langle b_i \, b_j \exp\,(i\mathbf{Q}.[\mathbf{r}_i(t) - \mathbf{r}_j(0)]) \rangle \; k_1 \, dk_1 \, d\Omega$$

$$= \frac{k_1}{k_0} \sum_{ij} \langle b_i \, b_j \exp\,(i\mathbf{Q}.[\mathbf{r}_i(t) - \mathbf{r}_j(0)]) \rangle \, d\omega_1 \, d\Omega \tag{4-10}$$

$$\frac{I}{I_0} = \frac{d^2\sigma}{d\Omega \, d\omega} d\Omega \, d\omega_1 = N \frac{k_1}{k_0} S(\mathbf{Q},\omega) \, d\Omega \, d\omega_1 , \tag{4-11}$$

with

$$S(\mathbf{Q},\omega) = \frac{1}{2\pi} \int_{-\infty}^{\infty} dt \exp\,(-i\omega t) \, I(\mathbf{Q},t) \tag{4-12}$$

and

$$I(\mathbf{Q},t) = \frac{1}{N} \sum_{ij} \langle b_i \, b_j \exp\,(i\mathbf{Q}.[\mathbf{r}_i(t) - \mathbf{r}_j(0)]) \rangle \; . \tag{4-13}$$

The double differential cross-section, $\frac{d^2\sigma}{d\Omega\, d\omega}$, represents the normalized scattered intensity per unit energy, per unit solid angle. I(Q,t) and S(Q,ω) are called the intermediate scattering function and scattering law, respectively. The molecular motion can be seen to be related to the scattering functions, by averaging explicitly the intermediate scattering function. Eq. (4-13) can be rewritten as

$$I(\mathbf{Q},t) = I_p(\mathbf{Q},t) + I_S(\mathbf{Q},t) \tag{4-14}$$

where

$$I_p(\mathbf{Q},t) = \frac{1}{N} \sum_{ij} b_i^{coh}\ b_j^{coh} \langle \exp\left(i\mathbf{Q}.[\mathbf{r}_i(t) - \mathbf{r}_j(0)]\right) \rangle , \tag{4-15}$$

$$I_S(\mathbf{Q},t) = \frac{1}{N} \sum_{i} (b_i^{incoh})^2 \ \langle \exp\left(i\mathbf{Q}.[\mathbf{r}_i(t) - \mathbf{r}_i(0)]\right) \rangle ; \tag{4-16}$$

furthermore,

$$S(\mathbf{Q},t) = S_p(\mathbf{Q},t) + S_S(\mathbf{Q},t) . \tag{4-17}$$

This can be done because the scattering length b_i is independent of its position. The scattering function S(Q,t) has two parts: coherent and incoherent. If the sample contains no hydrogen atoms, then the scattering is mainly coherent and $b_i^{coh} >> b_i^{incoh}$. If the sample contains hydrogen atoms, then the scattering is mainly incoherent and $b_i^{incoh} >> b_i^{coh}$. In our experiment, we are interested in incoherent scattering, which provides a unique and powerful probe in the analysis of the motions of protons and consequently of the dynamics of the macromolecule itself.

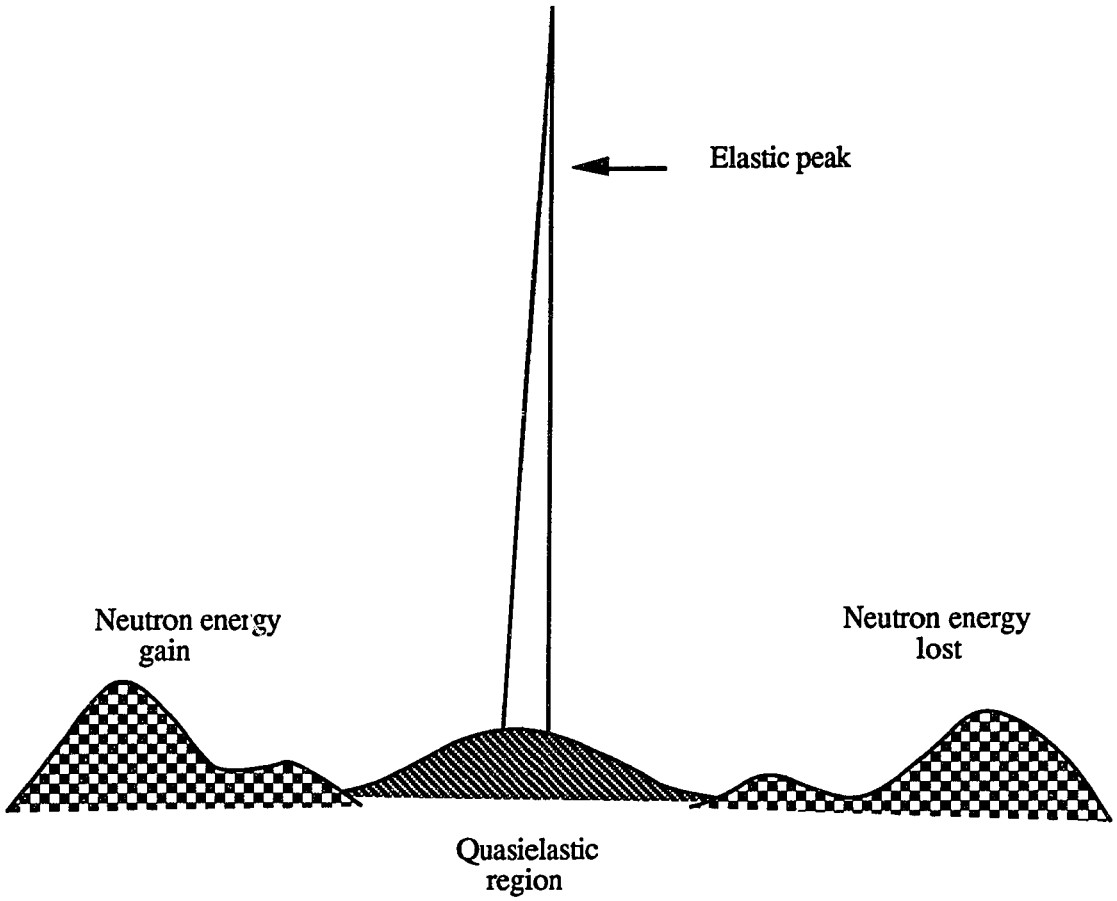

Fig. 2. Schematic diagram of experimental incoherent neutron scattering spectra: elastic, inelastic and quasielastic. Reproduced from Cusack (1989).

D. *Inelastic, Elastic and Quasielastic Scattering.*<14,23,24,25>

The incoherent scattering spectra can be divided into three regions: inelastic, elastic, and quasielastic (see Fig.2). The inelastic spectra contains regions of non-zero values of energy transfer. It gives details on the exchange of energy with vibrational modes in the molecule, and thus is an indispensable tool of vibrational spectroscopy. The elastic peak has information on the correlation in the atomic positions at infinite time. Thus, the more

restricted the nuclei are, the more intense is the elastic spectra . The quasielastic profile includes the region around $\omega=0$. It provides information on stochastic motions such as intramolecular barrier crossing events and over-damped vibrational modes. It is often modelled as a Lorentzian or the sum of Lorentzians.

E. *Incoherent Scattering from Hydrogenous Sample.*

For a single hydrogen atom, the incoherent scattering function is

$$I(\mathbf{Q},t) \approx I_S(\mathbf{Q},t) \propto \langle \exp(i\mathbf{Q}.[\mathbf{r}(t)-\mathbf{r}(0)]) \rangle. \quad (4\text{-}18)$$

Let $\mathbf{r} = \mathbf{d} + \rho + \mathbf{u}$; where $\mathbf{d}$ defines the molecular centre of mass (c.o.m.), ρ defines the position of the proton with respect to the c.o.m., and $\mathbf{u}$ stands for the vibrational displacement around the average position. In the classical approximation, we have:

$$\langle \exp i\mathbf{Q}.(\mathbf{r}-\mathbf{r}_0) \rangle = \langle \exp i\mathbf{Q}.(\mathbf{d}-\mathbf{d}_0) \exp i\mathbf{Q}.(\rho-\rho_0) \exp i\mathbf{Q}.(\mathbf{u}-\mathbf{u}_0) \rangle. \quad (4\text{-}19)$$

Assumming that translation, rotation, and vibration are uncoupled, Eq. (4-19) becomes

$$\langle \exp i\mathbf{Q}.(\mathbf{r}-\mathbf{r}_0) \rangle = \langle \exp i\mathbf{Q}.(\mathbf{d}-\mathbf{d}_0) \rangle \langle \exp i\mathbf{Q}.(\rho-\rho_0) \rangle \langle \exp i\mathbf{Q}.(\mathbf{u}-\mathbf{u}_0) \rangle, \text{ or}$$

$$I_S(\mathbf{Q},t) = I_S^{trans}(\mathbf{Q},t) \; I_S^{rot}(\mathbf{Q},t) \; I_S^{vib}(\mathbf{Q},t) . \quad (4\text{-}20)$$

After Fourier transforming (4-20), we have

$$S_S(\mathbf{Q},\omega) = S_S^{trans}(\mathbf{Q},\omega) \otimes S_S^{rot}(\mathbf{Q},\omega) \otimes S_S^{vib}(\mathbf{Q},\omega) . \quad (4\text{-}21)$$

where $\otimes$ represents the convolution. So when the motions are uncoupled, the scattering law is the convolution product of the scattering laws for three kind of motions<8,9,19,20,26>.

F. *Incoherent Quasielastic Scattering Spectra.*

1. Rotation:

For the case of isotropic rotational diffusion of a proton on a sphere of radius ρ, the probability distribution G_S of its orientation Ω is governed by

$$\frac{\partial G_S}{\partial t} = D_r \nabla^2_\Omega G_S \tag{4-22}$$

where $G_S(\Omega, \Omega_0, t)$ is the probability of finding the orientation Ω at time t if it was Ω_0 at t = 0. D_r is the rotational diffusion coefficient. ∇^2_Ω is the operator on Ω. The solution of this equation is

$$G_S(\Omega, \Omega_0, t) = 4\pi \sum_{l=0}^{\infty} \exp[D_r l(l+1)t] \sum_{m=-l}^{l} Y_m^l(\Omega) Y_m^{l*}(\Omega_0). \tag{4-23}$$

The intermediate scattering function becomes<19,20,27>

$$I(Q,t) = \frac{1}{4\pi} \int_{-\infty}^{\infty} dt \exp i\mathbf{Q}.(\rho - \rho_0)\, G_S\, d\Omega\, d\Omega_0$$

$$= J_0^2(Q\rho) + \sum_{l=1}^{\infty} (2l+1)\, J_l^2(Q\rho) \exp[-D_r l(l+1)t] \tag{4-24}$$

and

$$S(\mathbf{Q},\omega) = J_0^2(Q\rho)\,\delta(\omega) + \frac{1}{\pi} \sum_{l=1}^{\infty} (2l+1)\, J_l^2(Q\rho) \frac{D_r l(l+1)}{[D_r l(l+1)]^2 + \omega^2}, \tag{4-25}$$

Here the scattering law is composed of a sharp peak superimposed on a broadened component (a sum of Lorenztians) whose width is of the order of a few D_r and whose intensity depends on Q.

2. Translation:

For isotropic translational diffusion, the probability distribution is given by

$$\frac{\partial G_s}{\partial t} = D_t \nabla^2_d G_s , \qquad (4\text{-}26)$$

$G_s (\mathbf{d}, \mathbf{d}_0, t)$ is the probability of finding the particle at $\mathbf{d}$ at time t if it was at $\mathbf{d}_0$ at t = 0. D_t is the diffusional constant. ∇^2_d is the operator on d.

The solution for G_s can be found:

$$G_s (\mathbf{d}, \mathbf{d}_0, t) = (4\pi D_t t)^{\frac{-3}{2}} \exp [-\frac{(\mathbf{d} - \mathbf{d}_0)^2}{4 D_t t}] . \qquad (4\text{-}27)$$

The intermediate scattering function is :

$$I(\mathbf{Q},t) = \int_{-\infty}^{\infty} dt \exp i\mathbf{Q}.(\mathbf{d}(t) - \mathbf{d}(0)) G_s \, d\mathbf{d} \, d\mathbf{d}_0 = \exp (-D_t Q^2 t), \qquad (4\text{-}28)$$

and

$$S_s (\mathbf{Q},t) = \frac{D_t Q^2}{[D_t Q^2]^2 + \omega^2} . \qquad (4\text{-}29)$$

The line-width for this model varies as Q^2 <19,20,28>.

3. Vibration:

In the quasi-elastic region, the vibrational S (Q,ω) can be shown to be equal to the Debye-Waller factor exp(- $Q^2 <u^2>$), $<u^2>$ is the mean square vibration amplitude. This Debye-Waller factor plays an important role in protein dynamics, especially in the conformational substates concept introduced by Frauenfelder and others (see discussion in a later chapter). It should be pointed out that the above DW factor results from the assumption that the motion of the particles is unimodal and harmonic<7,19,21>.

V. Data Corrections and Fitting.

A. *Multiple Scattering.*

So far we have discussed the idealized situation in which the scattered neutron intensities are obtained from a detector with an infinite-resolution and a monochromatic incident beam. This is not the case in a real experiment and corrections must be made to compare data with the models. There are also other effects that make the data analysis more difficult, one of which is the effect of multiple scattering. Reallistically, the scattering law should include second and higher-order scattering-terms. However, the multiple scattering effect is complicated. It is advantageous if the effect can be avoided altogether; e.g., the effect can be made negligible by employing samples with high transmission. Before ignoring it, it is useful to see how multiple scattering depends on the physical features of the sample. For simplicity, let us look at a flat sample, thickness d and other dimensions large compared to the neutron beam. The mean free path of the neutron inside the sample is $l = \Sigma^{-1}$ where Σ is the total cross section per unit volume,

$$\Sigma = \Sigma_a + \Sigma_s , \tag{5-1}$$

and Σ_a is the absorption cross section, Σ_s is the scattering cross section per unit volume. In our hydrogenated sample, we can ignore Σ_a ($<< \Sigma_s$). For example, in the case of water H_2O, $\rho = 1$ g/cm^3, mw (H_2O) = 18g, σ_{incoh} (H) = 80 barns and σ_{incoh} (O) $\approx$ 0, we have

$$\Sigma_s = \Sigma_{incoh} = \frac{\rho}{mw\ (H_2O)} N_a\ (\sigma_{incoh}\ (O) + 2\sigma_{incoh}\ (H)\ ) \approx 5\ cm^{-1}. \tag{5-2}$$

N_a is the Avogadro number. Thus, the mean free-path in the sample is about 2 mm. A formula, developed by S. J. Cocking, gives the effect of second order scattering relative to the first order scattering as follows, given that S(Q) is independent of Q,

$$X(t,Q) = (\frac{t}{L}) \ln (\frac{L}{t}), \quad \text{for } t < L \tag{5-3}$$

where L is the mean free-path of neutrons in the sample,

t is the thickness of the sample,

X is the ratio of twice scattered intensity to once scattered intensity.

For S(Q) in the region of a maximum, at t = eL, X(t,Q) is independent of t. And X(t, Q) varies more slowly than t in all cases[29]. Thus, based on this formulation, the rough estimation of X(t, Q) for L= 2 mm shows that X<< 1. A Monte Carlo simulation study has been done by E. C. Trantham and D. Heidorn. The study concludes that the errors are about 10% in the line width and do not change much with Q. The amplitude, however, changes as much as 30% due to multiple scattering and fluctuates with Q[30].

B. *Inelastic Scattering.*

The contribution of inelastic scattering of the sample in the quasielastic regime requires careful analysis which takes into account the inelastic background. One way of estimating the inelastic contribution is to obtain the inelastic contribution spectrum experimentally and extrapolate it to the quasielastic range for correction purposes. In our case, we scan the quasielastic spectrum by varying ω and holding Q constant. The inelastic background is well represented by a simple linear function,

$$I_{\text{inel. bg.}} = A + B\omega . \tag{5-4}$$

The relative contribution of the inelastic background to the signal is approximately given as<8>

$$C = \frac{4.6 \times 10^{-5} Q^2 (0.77T + 1)}{1 + 4.6 \times 10^{-5} Q^2 (0.77T + 1)} \qquad (5\text{-}5)$$

where C is the ratio between the background and the signal. The above formula is derived from the single-phonon scattering law for a crystal.

Another contribution to the background is the sample holder. In previous experiments, a separate scan of the aluminum sample holder had been done, and it is sufficient to represent it by a linear function of ω as in the case of the sample itself.

In order to observe the dynamics of protons associated with the biomolecules, we placed them in a D_2O solution. The scattering from the D_2O in the solution also requires some corrections to the data. For small Q, the intermediate scattering function for coherent scattering (D_2O) can be approximated as<31>

$$F(Q,t) = \exp\left[- C_1 (Q)\, t - \frac{1}{2} C_2 (Q)\, t^2 \ldots \right] \qquad (5\text{-}6)$$

where C_1 (Q) is the term of immediate interest. In the frequency domain, this term transforms into a Lorentzian lineshape with Q-dependent width. For small t, the second term in the expansion is negligible. C_2 (Q) describes the deviations from exponential decay of the time correlation and gives a non-Lorentzian component. For D_2O, the coherent cross section is 80% of the total scattering cross section, so in the fitting, we require a second Lorentzian for the D_2O contribution. The fitting parameters were taken from a separate fit on the D_2O-only scans and these parameters were held fixed in the protein + D_2O scans fitting. The fitting gives smaller errors and chi-squared when the second Lorentzian for D_2O is included.

C. *Spectrometer Resolution Function.*

Before the data is analyzed, a few corrections must be done on the raw data. One of the corrections is the effect of slit smearing. This problem arises from the fact that the signal being detected is averaged over the geometry of the monochromator, collimator, and detector. Ideally, the instrument should have a source-monochromator-collimator combination which delivers perfectly monochromatic, infinitely collimated radiation which is directed through an infinitesimally thin specimen. The scattered neutrons then are registered by a detector with an infinitesimally small acceptance aperture. In reality, the beam has finite size, and even an ideal detector will be seeing scattered radiation over a range of angles. A less-than-perfect monochromatization of the beam has a similar effect. In all, the signal measured at scattering angle θ will not be $I(\theta)$ but some kind of weighted average over a range of angles $\theta \pm \Delta$. The signal measured is a distorted version of the signal desired. Mathematically, the effect of smearing the signal can be thought of as a convolution<8,9,32>.

$I_0(Q,\omega)$, the measured signal, is given as follows:<33>

$$I_0(Q,\omega) = \int_{-Q'}^{Q'} dQ_0 \int_{-\omega'}^{\omega'} d\omega_0 \; S_i(Q-Q_0, \omega-\omega_0) \; R(Q_0, \omega_0) . \qquad (5\text{-}7)$$

$R(Q, \omega)$ is the resolution in (Q, ω) space, and $S_i(Q, \omega)$ is the ideal signal. In our spectrometer, the width of the Q-resolution function is much smaller than any feature in a constant ω scan, except in the case of a Bragg peak. Thus for constant Q, the scattering law is averaged over a narrow range of Q-space in which $S_i(Q, \omega)$ is almost constant. So in this approximation, it can be shown

$$R(Q, \omega) \approx \delta(Q) R(\omega). \qquad (5\text{-}8)$$

Then (5-1) becomes

$$I_0(Q,\omega) = \int_{-\omega'}^{\omega'} d\omega_0 \; S_i(Q, \omega-\omega_0) \; R(\omega_0) . \qquad (5\text{-}9)$$

For convenience, the limits in (5-3) are usually taken to be $\pm \infty$.

Our resolution function was measured by scanning the elastic incoherent peak from vanadium. It should be noted that the resolution is not symmetric about $\omega = 0$, due to the fact that the final wave vector k_F is varied<34,35>. Taking the variation of k_F into account, the $R(\omega)$ has approximately a Gaussian form in ω multiplied by a skew factor, <36>

$$R(\omega) \propto (A - B\omega) \exp(-\frac{\omega^2}{K^2}) \; , \text{ where } K = \frac{\Gamma_r}{2\sqrt{\ln 2}}$$

Γ_r is the resolution full-width-half-maximum, A and B are arbitrary constants.

D. *Voigt Function.*<36-41>

Using the above mentioned resolution function, we can write $I_0(Q,\omega)$ explicitly as,

$$I_0(Q,\omega) = \frac{1}{K\sqrt{\pi}} \int_{-\omega'}^{\omega'} d\omega_0 \; S_i(Q, \omega-\omega_0)(A - B\omega_0) \exp(-\frac{\omega^2}{K^2}) \exp(-Q^2\frac{\langle u^2\rangle}{3}). \qquad (5\text{-}10)$$

In some models used to describe the dynamics of protons in solution, the shape of $S_i(Q, \omega)$ is Lorenztian, including the model we used to describe our system. So $S_i(Q, \omega)$ takes the form

$$S_i(Q, \omega) = \frac{1}{\pi\hbar} \frac{\Gamma/2}{(\Gamma/2)^2 + (\omega-\omega_0)^2} \qquad (5\text{-}11)$$

Then the experimental spectrum is:

$$I_0(Q,\omega) = \frac{1}{K\hbar\pi^{3/2}}\int_{-\omega'}^{\omega'} d\omega_0 \,(A - B\omega_0)\exp\left(-\frac{\omega_0^2}{K^2}\right)\exp\left(-Q^2\frac{\langle u^2\rangle}{3}\right)\frac{\Gamma/2}{(\Gamma/2)^2+(\omega-\omega_0)^2} \quad (5\text{-}12)$$

Using the definition of the complex Voigt function, we have

$$\int_{-\infty}^{\infty} dt \frac{y\exp(-t^2)}{(x-t)^2+y^2} = \pi\,\Re e\,V(x+iy) \quad (x \text{ is real}, y>0). \qquad (5\text{-}13)$$

It can be shown that $I_0(Q,\omega)$ can be approximately written as,

$$I_0(Q,\omega) = \frac{1}{K\hbar\sqrt{\pi}}\exp\left(-Q^2\frac{\langle u^2\rangle}{3}\right)[1-C\omega]\,\Re e\left\{V\left(\frac{\omega}{K}+i\frac{\Gamma(Q)}{2K}\right)\right\}, \qquad (5\text{-}14)$$

where $C \approx .02$, a small correction, so it is permissible to assume the resolution function is an ideal Gaussian in which $I_0(Q,\omega)$ has the form

$$I_0(Q,\omega) = \frac{1}{K\hbar\sqrt{\pi}}\exp\left(-Q^2\frac{\langle u^2\rangle}{3}\right)\Re e\left\{V\left(\frac{\omega}{K}+i\frac{\Gamma(Q)}{2K}\right)\right\}. \qquad (5\text{-}15)$$

As shown later on, the fits done with both forms of resolution functions (5-14) and (5-15) are approximately of equal quality, within the error bars. The numerical values of the Voigt function can be found by Taylor series expansion, or by asymptotic series expansion, or by numerical integration. The Voigt function is also related to the error function by

$$V(z) = \exp(-z^2)(1-\mathrm{erf}(-iz)), \text{ and} \qquad (5\text{-}16)$$
$$\mathrm{erf}(z) = \frac{2}{\sqrt{\pi}}\int_0^z dt \exp(-t^2).$$

E. *Fitting Techniques for the Voigt Function.*

In principle when one of the two contributions to the experimental spectrum is known, e.g. the resolution function, then the other can be obtained through Fourier deconvolution. This procedure can go wrong if the transform of the response function is exactly zero for some values of R_n - the values for the experimental spectrum - since we can not divide by these. This shows that during the convolution, the information was lost at that one frequency so that a deconvolution of that frequency component is not possible. This procedure is also quite sensitive to noise in the input data, and to the accuracy of the known response function. It requires excellent statistics in the data set for success. So a perfectly reasonable deconvolution procedure sometimes produces nonsense.

An alternate approach is an approximation to the Voigt line shape using a linear combination of Gaussian and Lorentzian curves. The useful range of the approximation includes the lines sharper than a Lorentzian and lines flatter at the top than a Gaussian. The approximation can be written as

$$F(\Gamma, \eta, x) = \frac{\eta}{1 + (\frac{x - x_0}{0.5\Gamma})} + (1 - \eta) \exp\left(-\frac{x - x_0}{b\Gamma}\right)^2. \qquad (5\text{-}17)$$

In the study of hydrated proteins, H. D. Middendorf and Sir J. Randall[49] have applied this technique successfully as compared to using the complete Voigt function. In this fit, the width of the experimental line shape Γ is known but not the width of the Lorentzian and the Gaussian. However, from the tabulated data in ref. 37, we can find the width of the Lorentzian and of the Gaussian respectively.

Our approach is different from the above two mentioned methods. Using the numerical values of the Voigt line shape, the experimental spectrum is fitted by a non-linear

least-square method developed by Marquardt. The guess for each parameter in the fitted model is given initially by the user. The fitting algorithm then calculates the chi-square,

$$\chi^2 \equiv \sum_{i=1}^{n} \left(\frac{y_i - y\,(x_i ; a_1 \ldots a_m)}{\sigma_i} \right)^2 \qquad (5\text{-}18)$$

If the guess is good, the jump from the current trial parameters a_{cur} to the minimizing ones a_{min} occurs in one step,

$$a_{min} = a_{cur} + D^{-1}.[\, -\nabla\chi^2 (a_{cur})] \qquad (5\text{-}19)$$

where D^{-1} is related to the Hessian matrix, namely the second partial derivative of χ^2 with respect to the parameters a_k and a_l. However, if the guess is a poor estimate to the parameters of the model, we can take a step down the gradient as in the steepest descent method:

$$a'_{cur} = a_{cur} - \text{ constant } .[\, \nabla\chi^2 (a_{cur})]. \qquad (5\text{-}20)$$

The algorithm repeats the procedure until χ^2 and the parameters converge to a stable equilibrium in the parameter-space. In order to test the goodness of the fit, several procedures are used:

– several sets of initial guesses of parameters were used to check the convergence of the algorithm.

– minimization of the number of free parameters whenever possible, to reduce the dimensions of free parameter space, which is likely to reduce the "false" local minima that the fits might converge to.

VI. Neutron Spectrometer.

A. *Production of Neutrons.*

In the nuclear reactor, neutrons are produced by fission. As they collide with the moderators, the neutrons lose some of their energy. At some distance from their origin, they come to thermal equilibrium with the moderator and the beryllium reflector. These neutrons are then transfered to the experimental sites by beam tubes. The energies of these neutrons cover a wide range. In order to perform diffraction experiments, the beam needs to be monochromatized. One way of achieving monochromatization is Bragg reflection of the beam from crystal planes; the favorite crystal for this purpose is pyrolitic graphite because of its high reflectivity coefficient. The Bragg scattering law states $\lambda = 2\, d_{hkl} \sin\theta$, where $\lambda = \frac{h}{mv}$ is the neutron wavelength, d_{hkl} the distances between lattice planes, θ the diffraction angle. A Bragg diffraction, however, would also need an appropriate filter to produce a true monochromatic beam, since more than one λ can satisfy the Bragg's law at fixed θ. Usually, a polycrystalline filter is chosen such that the largest λ_{max} is selected. The cost of this procedure is a reduction in intensity of the neutron beam. The final energy E_f of the scattered neutrons must be analyzed to determine the energy change of the scattered neutron.

Another method often used in a TOF (Time-of-Flight) spectrometer is a velocity selector. The main components of the selector consist of a cylindrical rotor to chop the beam and select a desired velocity for the neutrons used, and a helical channel to guide the monochromatized beam. This way, however, is very costly in neutron intensity. Monochromatization using crystals is more cost effective. However, it has some disadvantages. First, to change neutron wavelength requires elaborate realignment of the apparatus. Then there is a limit on what maximum wavelength can be obtained. It is also costs valuable flux due to its less than perfect reflective feature<44>.

B.*Triple-Axis Spectrometer at BNL (Brookhaven National Laboratory), H8.*

Our experiment was done at BNL on the H8 triple-axis spectrometer (see Fig.3). H8 is primarily used for single crystal inelastic neutron scattering experiments. However, as in our case, it can also easily be adjusted to quasielastic scattering experiments. It is equipped with a monochromator housing that can hold either a PG (002) or a Heusler crystal, for unpolarized and polarized neutron experiments respectively. The incident energy can be varied so scans with a fixed final energy can be obtained, or a fixed incident energy with varied final energies can also be utilized. Cooled Be and pyrolytic graphite crystals are available for removing higher order beam contamination. The sample table is equipped with a manual two-axis goniometer with a $\pm 10^0$ range and is compatible with a variety of available cryostats and furnaces. External collimation is provided by Soller slits with 5x5 cm^2 cross section.

H8 Station Parameters.

Flux at monochromator position (20' in-pile collimation)	4.2×10^9 n/cm^2 sec
Monochromator scattering angle	$10^0 < 2\theta_M < 75^0$
E_0 or λ_0 (PG 002)	$4.9 < E_0 < 240$meV
	$4.1 < \lambda_0 < 0.58$Å
Beam size	5 (h)x3.1 (w) cm^2
Sample scattering angle	$45^0 < 2\theta_S < 140^0$
Analyzer scattering angle	$-100^0 < 2\theta_A < 100^0$
In-pile collimation	10',20',40'
External collimation	10',20',40'
Detector	BF_3

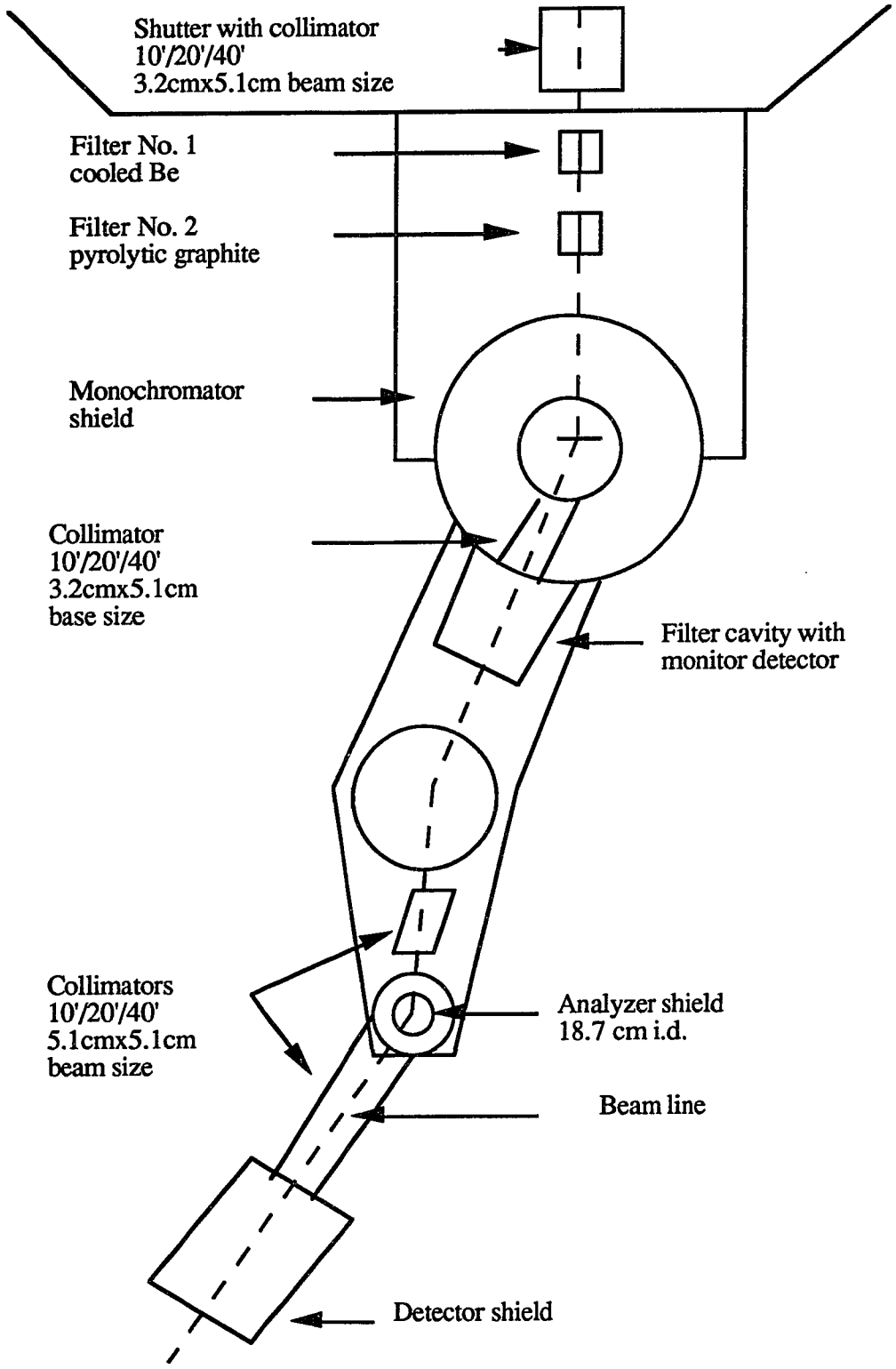

Fig. 3. Schematic plan of triple-axis spectrometer installed at H8.

VII. The Effect of Solvent Molecules on Protein Dynamics.

The dynamics of proteins are directly coupled with their environment: the solvent molecules, in most cases, are water. Water is an important factor in all living organisms. Many functional and structural details of its interaction with biological molecules have been investigated by a variety of techniques ranging from calorimetry to magnetic resonance. These have shown that a small number of water molecules are tightly bound in the interior of the protein and can be regarded as an essential part of its tertiary and quartenary structure (see Fig.4 for basic structures of the protein). A number of these water molecules are loosely bonded but still localizable at or near the biomolecule's surface.

Based on motional information on protein hydration at the molecular level from different spectroscopic techniques, the water molecules can be classified into different classes according to their characteristic rotational diffusion time τ_r . First, a small number are bound almost irrotationally ($\tau_r = 10^{-5}$ to 10^{-2} s) at specific hydration sites with multiple hydrogen-bonds. Secondly, a large number interact less strongly with the biomolecule but are still sufficiently restricted so that $\tau_r \approx 10^{-9}$ s. Other water molecules that have motional properties similar to bulk water are the third type ($\tau_r = 10^{-10}$ to 10^{-11} s). With our lyophilization procedure used on the trypsin, where the loosely bounded water molecules are exchanged with D_2O molecules, most of the water molecules closely associated with the trypsin likely remain intact<49>.

The solvent molecules have been shown to influence the dynamical properties of proteins. These effects are not simply due to solvent viscosity, but also due to protein-solvent interactions. In effect, the protein molecule also plays a role in solvent dynamics and structure. For example, the water molecules around charged, polar, and apolar sidechains have significantly different diffusion coefficients, and they exhibit different structures. A study of Polyox/water by D. Bearden indicated that in the presence of polym-

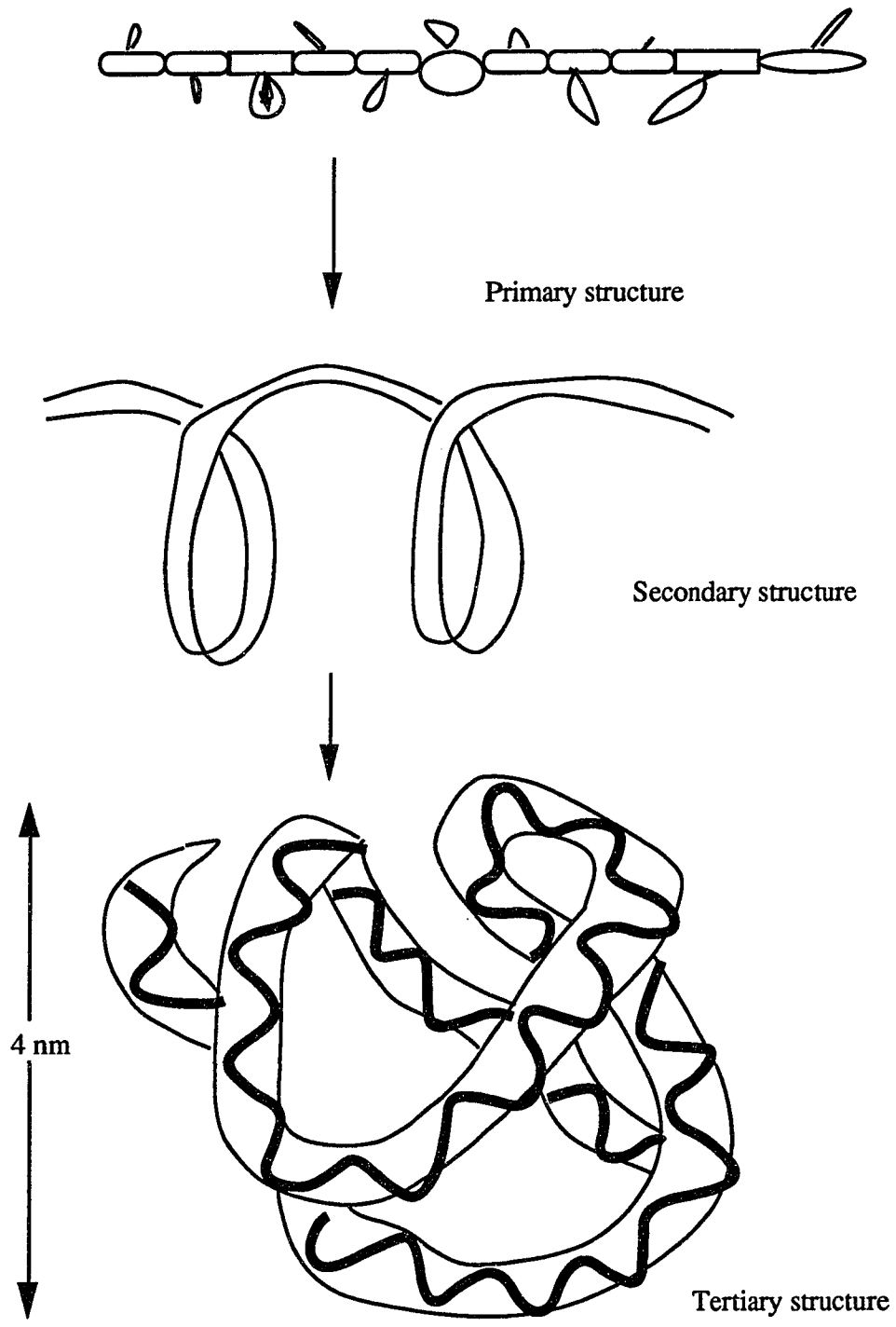

Fig. 4. Protein basic structures. Reproduced from Frauenfelder (1991).

er, H_2O hydrogens have a reduced diffusion coefficient and an increased residence time compared to pure water. QNS studies by Trantham et. al. on cysts of the brine shrimp (Artemia) and 20% agarose gels in H_2O and D_2O show the reduction of the motional freedom of intracellular water due to interaction with biomolecules<50,51,52>. The question of how the solvent molecules influence the protein motion is more difficult. In determining the effect of proteins on the motion of solvent molecules, we study the solvent system and solvent + protein system. The effect of the solvent on protein motions is less obvious due to the fact that we do not know how the protein behaves without the solvent molecules. It is quite reasonable to say that the protein is "dead" without the solvent. As the percentage of solvent molecules increases, the protein becames alive, the motions changing from local vibration to large amplitude diffusive motion.

VIII. Jump Diffusion Dynamics.

A. *The Relevance of Jump Diffusion Dynamics.*

We seek to explain the motion associated with the biomolecules, in our case trypsin, using the jump diffusion theory. There are several reasons for using the jump diffusion theory:

– previous experiments in our group have shown in general the experimental data revealed a similar behavior to that predicted by jump diffusion theory.

– the motion of the particles described by the theory is physically reasonable.

– the theory has been used to explain dynamics of systems similar to the system we study.

Before going into the details of jump diffusion theory, we first look at the inadequacy of continuous diffusion at large values of momentum tranfer Q, or small space-time values. The continuous diffusion theory predicts a rms velocity $\sqrt{v^2}=\sqrt{\frac{<r^2>}{t^2}} \propto t^{-0.5}$, so for t small the rms velocity becomes physically unreasonable. This theory is indeed only applicable to the continuum; the motion of particles under the influence of their neighbors requires a different theory, jump diffusion theory<46>.

B. *Jump Diffusion Theory.*

In explaining the details of this theory, we follow an approach<47> motivated by the paper of Hall and Ross (1981). The advantage of this approach is its simplicity. The method also introduces a parameter (jump length distance) that facilitates comparision with experiment. Historically, the first continous diffusion model for H_2O was proposed by Bernal and Fowler (1933) and later modified by Lennard-Jones and Pople (1951). This model later was proven to be inadequate on the basis of neutron scattering experiments by Brockhouse (1959)<48>. This opened the way for a jump diffusion theory, in which the

basic repeated mechanisms of a particle consist of a residence time and a diffusive time. We first assume the jump diffusion is a Markovian process, where successive jumps are not related, the spatial distribution of jump lengths is governed by $\rho(\mathbf{r})$, and its temporal distribution is a Poisson type.

1. Spatial distribution.

We assume the jumps are isotropic, with a spatial distribution that obeys the following conditions:

$$\rho(\mathbf{r}) = \rho(r), \tag{7-1}$$

$$\int_0^\infty \rho(r)\, d\mathbf{r} = 1, \tag{7-2}$$

$$\int_0^\infty r^2 \rho(r)\, d\mathbf{r} = \langle r^2 \rangle. \tag{7-3}$$

A number of possible forms for $\rho(r)$ will be considered below.

2. Temporal distribution.

The probability of m jumps in the time t is a Poisson process,

$$P_m = \frac{(t/\tau)^m}{m!} \exp(-\frac{t}{\tau}), \tag{7-4}$$

where τ is the mean oscillation life time of a particle at a site.

3. Self-correlation function.

We write the self-correlation function as,

$$G_s(\mathbf{r},t) = \sum_{m=0}^{\infty} R_m(\mathbf{r}) P_m(t), \tag{7-5}$$

where $R_m(\mathbf{r})$ = m-fold convolution of $\rho(r)$ with itself

$$= \rho^*\rho^*\rho^* \ldots \text{ m times} = \rho^{m*}. \tag{7-6}$$

The intermediate scattering function is:

$$I_S(Q,t) = \int G_S(r,t)\, \exp(i\, Q.r)\, dr = FT\,[G_S(r,t)] = FT\,[\sum_{m=0}^{\infty} \rho^{m*}\, P_m(t)\,. \qquad (7\text{-}7)$$

According to the Faltung theorem, we can write

$$FT\,[\,f*g*h\,] = (FT\,f)\,(FT\,g)\,(FT\,h)\,,\ \text{so}$$

$$FT\,\rho^{m*} = (FT\,\rho)^m = [\,F(Q)\,]^m,\ \text{where } F(Q) \text{ is the FT of } \rho(r) \qquad (7\text{-}8)$$

We can rewrite the intermediate scattering function,

$$I_S(Q,t) = \sum_{m=0}^{\infty} [\,F(Q)\,]^m \frac{(t/\tau)^m}{m!} \exp(-\frac{t}{\tau})$$

$$= \exp\,(-[\,1-F(Q)]\frac{t}{\tau}\,) = \exp\,(-\Gamma(Q)\frac{t}{\tau}\,). \qquad (7\text{-}9)$$

The scattering law is then,

$$S_i(Q,\omega) = \int I_S(Q,t)\, \exp(i\,\omega t)\, dt$$

$$= \frac{1}{\pi}\,\frac{\Gamma/\tau}{(\Gamma/\tau)^2 + \omega^2},\ \text{where } \Gamma/\tau \text{ is the width.} \qquad (7\text{-}10)$$

4. Different spatial distributions.

We will consider some possible forms for the jump distribution $\rho(r)$.

a. Gaussian.

$$\rho(r) = \frac{1}{(r_0\sqrt{2\,\pi})^3}\,\exp(-\frac{r^2}{2r_0^2})\,, \qquad (7\text{-}11)$$

$$F(Q) = \int \rho(r)\, \exp(i\, Q.r)\, dr = \exp(-\frac{r_0^2\, Q^2}{2})\,,$$

$$\frac{\Gamma}{\tau} = \frac{1}{\tau}(\,1-F(Q)\,)$$

$$= \frac{1}{\tau}(\,1-\exp(-\frac{r_0^2\, Q^2}{2})\,). \qquad (7\text{-}12)$$

b. Exponential A.

$$\rho(r) = \frac{1}{4\pi r_0^2 r}\,\exp(-\frac{r}{r_0}),\ \text{using the same procedure as above,} \qquad (7\text{-}13)$$

$$F(Q) = \frac{1}{1 + Q^2 r_0^2}\,,$$

$$\frac{\Gamma}{\tau} = \frac{1}{\tau}\left(1 - \frac{1}{1 + Q^2 r_0^2}\right) = \frac{1}{\tau}\left(\frac{Q^2 r_0^2}{1 + Q^2 r_0^2}\right). \quad (7\text{-}14)$$

c. Exponential B.

$$\rho(\mathbf{r}) = \frac{1}{4\pi r_0^2 r^2} \exp\left(-\frac{r}{r_0}\right), \quad (7\text{-}15)$$

$$F(Q) = \frac{1}{Qr_0} \tan^{-1}(Qr_0),$$

$$\frac{\Gamma}{\tau} = \frac{1}{\tau}\left(1 - \frac{1}{Qr_0} \tan^{-1}(Qr_0)\right). \quad (7\text{-}16)$$

d. Dirac-delta.

$$\rho(\mathbf{r}) = \delta(r - r_0), \quad (7\text{-}17)$$

$$F(Q) = \frac{1}{Qr_0} \sin(Qr_0),$$

$$\frac{\Gamma}{\tau} = \frac{1}{\tau}\left(1 - \frac{1}{Qr_0} \sin(Qr_0)\right). \quad (7\text{-}18)$$

In all cases, the width is $\sim Q^2$ (classical diffusion) for $Qr_0 << 1$, and Γ approaches constant for $Qr_0 >> 1$.

IX. Data Analysis and Discussion.

Our experiments were carried out on D_2O, trypsin powder, trypsin + D_2O (refer to chapter II for further details). The background scans on the D_2O were done to allow proper extraction of the real line shape of the scattering by the trypsin molecule. It turns out there is more than one way to remove the background from the data. One way is point-by-point subtraction. This method, however, introduces large statistical errors and thus affects the true line-width. The chosen technique is to fit the background with a reasonable model, in this case a Voigt function (see earlier chapter). All the parameters obtained from the D_2O fits are then fixed in the fitting of the trypsin + D_2O profiles. The exact form of the total scattering cross section is as following,

$$S(Q,\omega) = A + B\omega + L(D_2O)*R(\omega) + L(\text{trypsin} + D_2O)*R(\omega).$$

The $S(Q,\omega)$ spectra for D_2O was almost flat at high Q's (see appendix), and at low Q's there is a small quasielastic peak, which is well fit with a Voigt function. A fit at $Q=1.5$ Å^{-1}, T=300K is shown in Fig.5 (the points with error bars are experimental data; the x's are points from the fitting function.) The resolution function of the triple-axis spectrometer was fitted with two forms: a gaussian, and a supposedly more exact form, a gaussian multiplied by a skew parameter (as discussed in chapter V). The results from the fitting show that both forms are closely in agreement (within the error bars), with the resulting widths from the skew-gaussian larger (see Figs.6 & 7 where ◊ = gaussian). From the line shape of the width Γ/τ versus Q^2 in principle one should be able to obtain the details of the diffusive properties of the protons. In terms of jump-diffusion theory, one can measure the jump-length distribution $\rho(r)$, which in general is assumed to be gaussian (e.g. in X-ray scattering of biomolecules), but which could be different in the case of trypsin. One way to

FIG.5. Q=1.5 T=300K TRYPSIN + D2O FIT & DATA

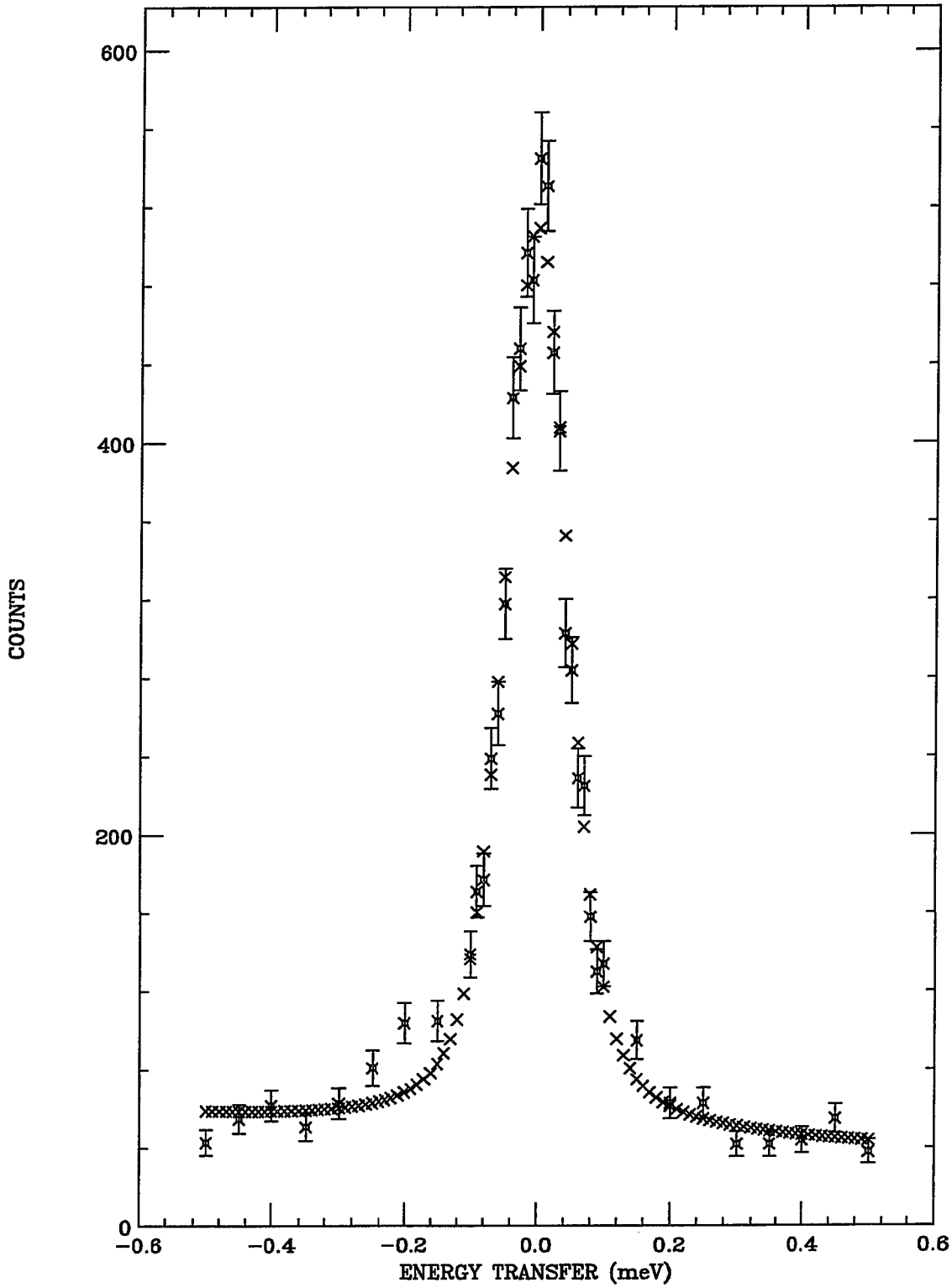

FIG.6. TRYPSIN + D2O SOLUTION AT T=300K

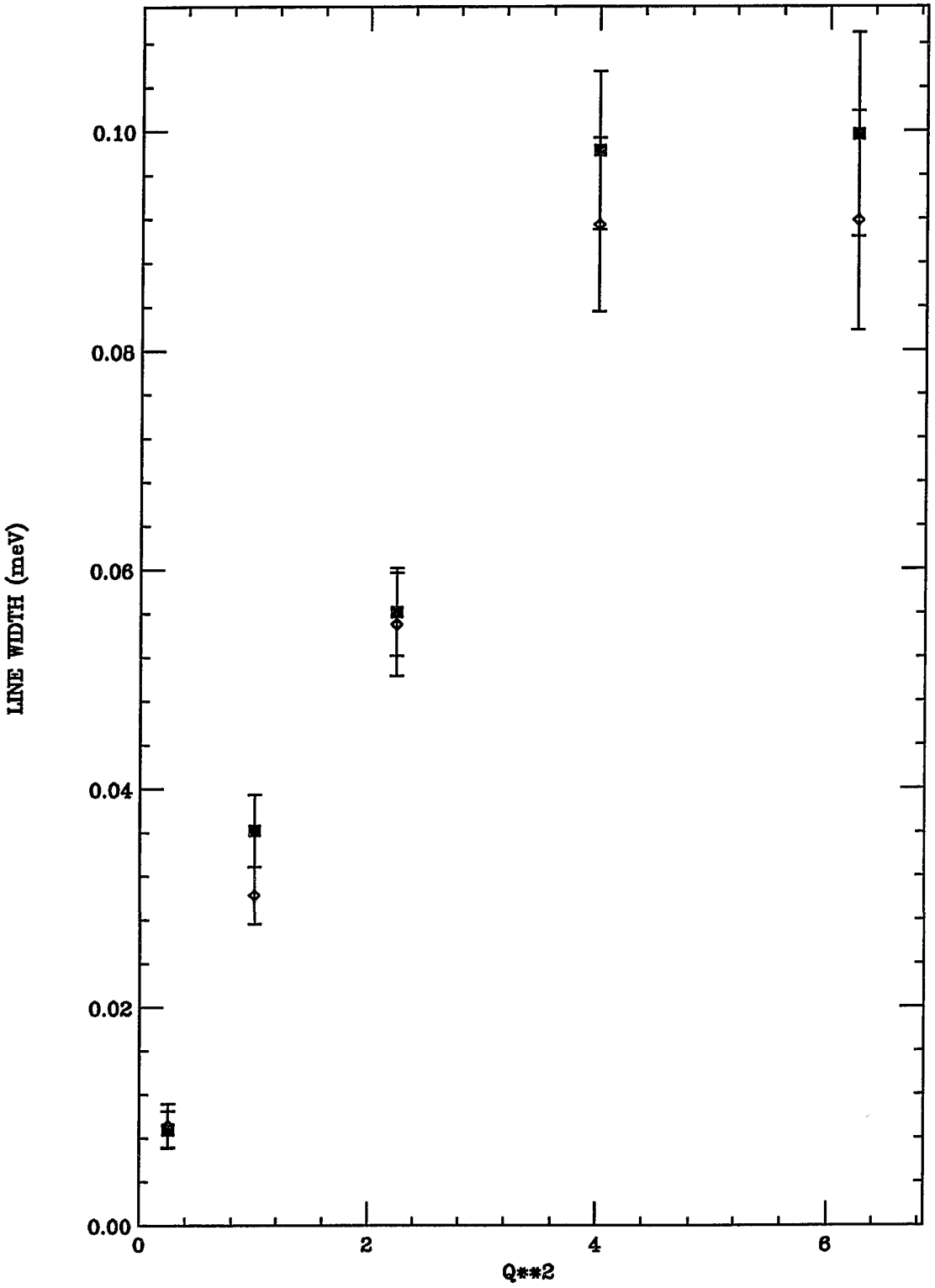

FIG.7. TRYPSIN + D2O SOLUTION AT T=280K

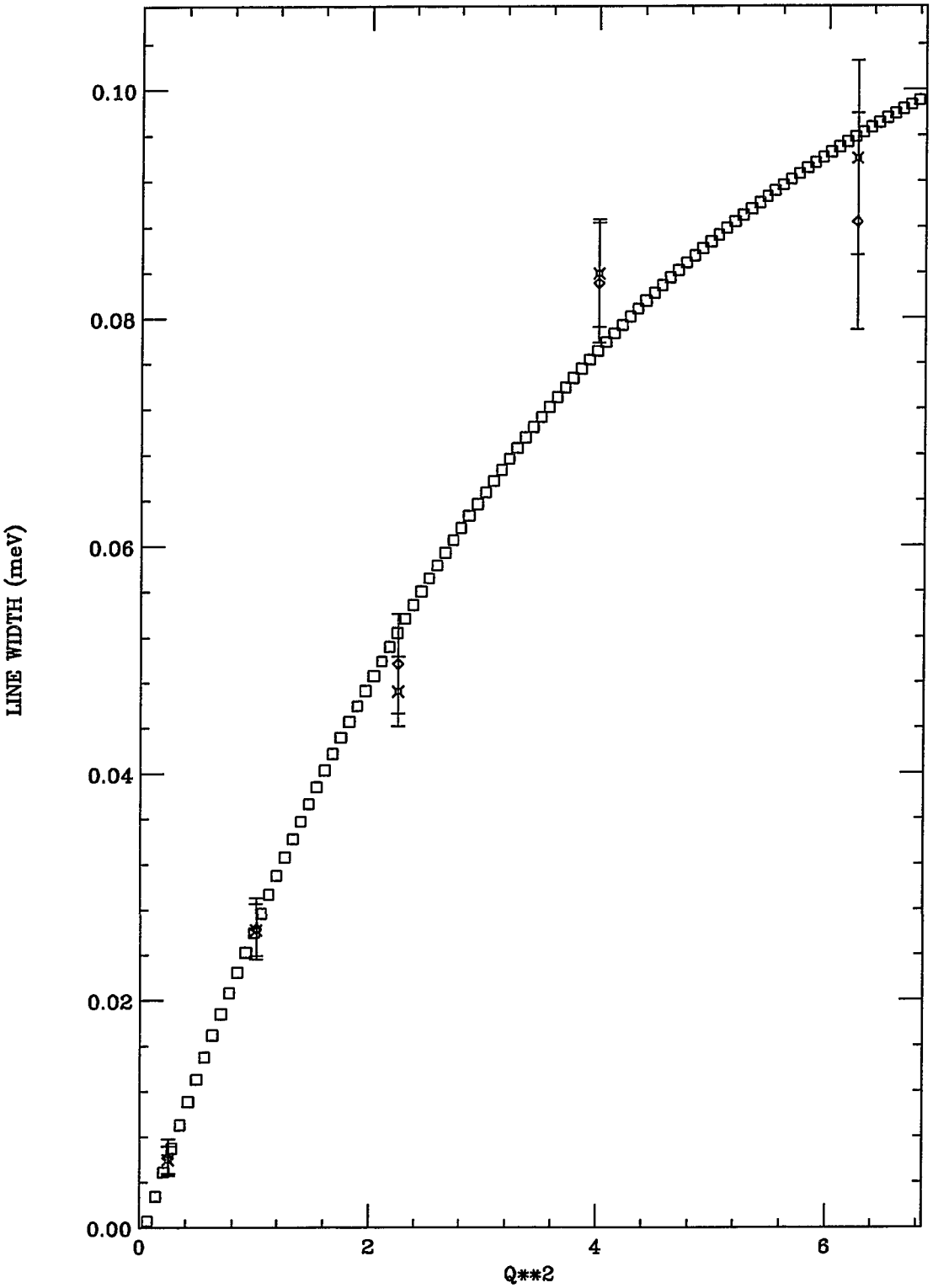

extract the information on the $\rho(\mathbf{r})$ is to work out the Q-dependent line-width from an assumed model and then fit the data with this function (as is done in the jump-diffusion theory section). Another way is to obtain a good set of data with better statistics, and inverse-fourier-transform the data to obtain the jump-length distribution $\rho(\mathbf{r})$. With the data available, we are only able to derive $\rho(\mathbf{r})$ by assuming a reasonable jump-diffusion model and fitting the data with a derived line-width versus Q^2 function. The line-width as a function of Q^2 for the trypsin + D_2O solution at 300K and 280K are shown in Fig.6 and Fig.7 . The line shapes are similar at both temperatures. They are linear at small Q^2 and level off at large Q^2 , which is characteristic of a jump-diffusion process. The leveling off is, however, based only on one point at Q=2.5 $Å^{-1}$.(See App. B for our most recent data in which more complete results are given for $\Gamma(Q^2)$). Thus we have only a tentative conclusion: the protons associated with the trypsin molecule perform some type of jump-diffusion. It is possible that the protons are also jumping between conformational substates as suggested by Frauenfelder. Since we have already exchanged out the loosely bound water molecules, the rearrangements of the more-tightly-bound water protons under study is closely associated with the motion of various trypsin segments. The exact jump-diffusion mechanism of these protons is uncertain at this time. The following quantitative discussion of the data is based on the jump-diffusion model: (model 4b. of Sect. VIII B)

$$\Gamma(Q) = \frac{2Q^2D}{1 + Q^2D\tau_0} .$$

The slope of the curve at small-Q values gives a diffusion coefficient of D = 0.18(± .019)x10^{-5} cm^2/sec, and the leveling off at large Q gives the residence time τ_0 = of 4.7(±1.3) x 10^{-11} sec at T = 300K. At T = 280K, we have D = 0.14(± .017) x 10^{-5} cm^2/sec, and τ_0 = 3.9(±.56) x 10^{-11} sec. For pure water, D is about 2.5 x 10^{-5} cm^2/sec, and τ_0 is approximately 2 x 10^{-12} sec. The results at 300K and 280K are consistent with

one another, with slightly smaller values of D and τ_0 at lower temperature, and with smaller D and longer τ_0 compared to the values for pure water. The residence time τ_0 of the hydrogens can be interpreted as the average lifetime of these hydrogens in their conformational substates. The similar previous experiments done by C. Lin at ONRL are not readily compared to ours because of his background problem, which caused a large statistical error on the data fitting after point-by-point background subtraction. One thing we can conclude with certainty is that the continous diffusion model is not compatible with the motion of the system in our study.

The Debye-Waller factor gives the average mean-square vibration amplitude for the hydrogens associated with the trypsin molecule. The main effect of the DW factor is a reduction in the peak intensity at high momentum transfer Q. The basic assumption, contained in the following equation:

$$S(Q,\omega=0) \sim \exp\left(-Q^2 \frac{\langle u^2 \rangle}{3}\right),$$

is that the probability of finding an atom a distance x from its equilibrium position due to its high-frequency-thermal motion is isotropic, and is a gaussian. Here the mean-square vibration amplitude $\langle u^2 \rangle_{QNS}$ measured by QNS is different from the mean-squared amplitude $\langle u^2 \rangle_{X\text{-}ray}$ measured by X-ray methods, which is defined as

$$\langle u^2 \rangle_{X\text{-}ray} = \langle u_v^2 \rangle + \langle u_{cs}^2 \rangle + \langle u_{ld}^2 \rangle .$$

$\langle u_v^2 \rangle$ represents the local atomic vibration (the same as $\langle u^2 \rangle_{QNS}$). $\langle u_{cs}^2 \rangle$ gives the contribution of the transitions between conformational substates. $\langle u_{ld}^2 \rangle$ is due to lattice disorder[53].

FIG.8. DEBYE–WALLER FACTOR TRYPSIN + D2O T=300K

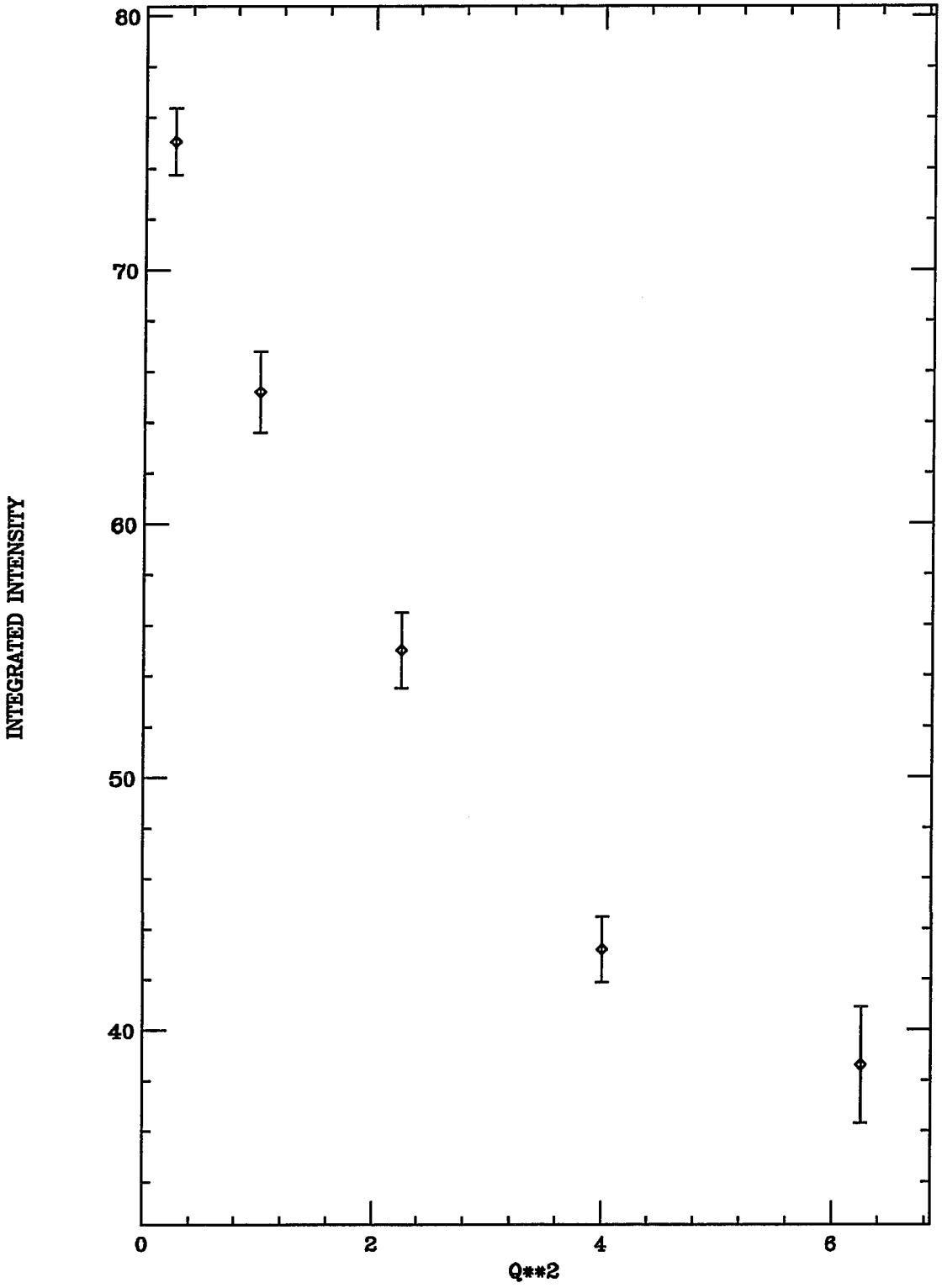

The DW factor to the integrated intensity of trypsin in D_2O at 300K is shown in Fig.8. The fit result gives $\frac{<u^2>}{3}$ = 0.33 Å^2. Computer simulation results give a value for the average $<u_v^2> + <u_{cs}^2>$ between 0.28 Å^2 and 0.36 Å^2. X-ray diffraction experiments give a value of the average $<u_v^2> + <u_{cs}^2> + <u_{ld}^2>$ between 0.48 Å^2 and 0.58 Å^2. According to a computer simulation on trypsin by McCammon, the averaged mean-square-amplitude of localized fluctuations is 0.46 Å^2 <54>. This value is approximately one-half of our experimental value $<u^2>$ = 0.99 Å^2 at 300K.

The fits of the DW factor for trypsin in D_2O at 280K and for trypsin powder using the same model are less successful (see Fig.9 & 10). The previous experiment done by C. Lin also shows a poor agreement with the DW model at 300K and 280K. One would like to think the problem lies in the data and its analysis, thus still believing the DW model is adequate to explain the high frequency vibrations of the system under study. This leaves the possibility of further experiments to verify the DW model. Or the DW model may be inadequate in this case. It is possible that the integrated intensity obtained experimentally indicates a non-linear fluctuation which can not be analyzed with a DW factor, which assumes a gaussian distribution of fluctuations around one conformation<7>.

The fit to the DW factor at room temperature T=300K is very satisfactory. The fits to the DW factor of data at lower temperature T=280K and of powder trypsin are less successful. It is possible that the effect is due to the reorientation of the trypsin hydrogens. At room temperature, the effect of rotational motion is negligible, since the molecules are less confined, and translational diffusive motion is dominated. At lower temperature and in the powder, the rotational effect becomes more visible. Thus the scattering law has term(s) due to rotational motion $J_0^2(Q\rho)\exp(-Q^2\frac{<u^2>}{3})$ and possible contributions from higher order Bessel functions<8> which are counted as part of the DW factor in our analysis. The disagreement seen in the experimentally determined $<u^2>$ and some of the molecular dynamics results could be due to rotational motion as described above.

FIG.9. DEBYE–WALLER FACTOR FOR TRYPSIN + D2O T=280K

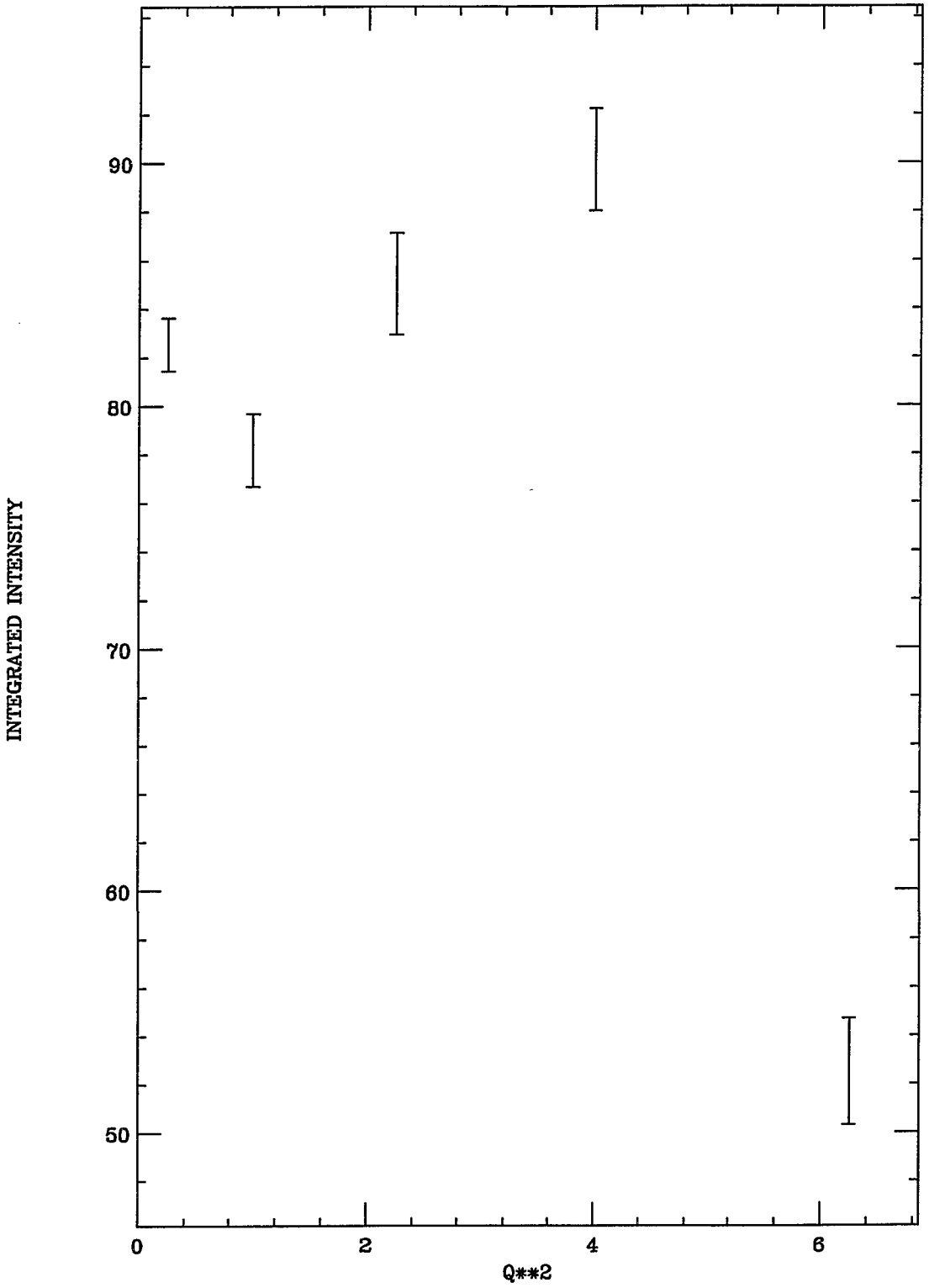

FIG.10. DEBYE–WALLER FACTOR POWDER TRYPSIN T=300K

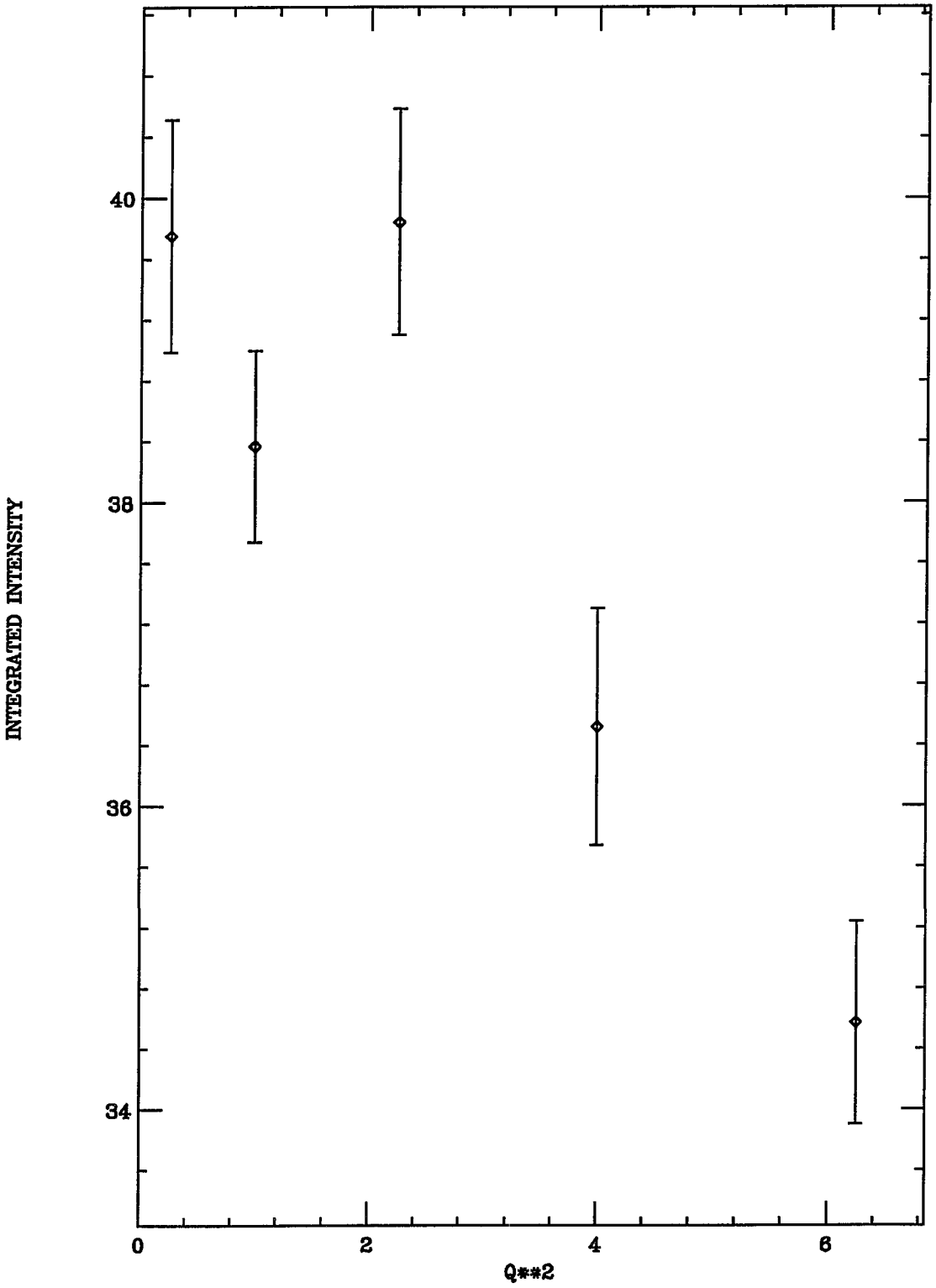

The frozen trypsin in D_2O at 200K does not indicate any broadening due to diffusive motion, showing a width equal to the spectrometer resolution function. The data collecting time-limitation allowed us to obtain data at only three values of Q. The thermal vibrational amplitude $\frac{\langle u^2 \rangle}{3} = 0.28\ \text{Å}^2$, but it has a large uncertainty.

In the low-resolution experiment, the S(Q) for pure D_2O at 300K shows a broad peak at about 2 Å^{-1}, as expected (see Fig.11). In trypsin + D_2O at 300K, the same peak is also present but is slightly less intense than for pure D_2O (see Fig.12). The intensity, in geneal, decreases with Q^2, an effect of the DW factor. However, the corrections due to background and inelastic scattering are difficult to assess, so there is a large uncertainty in determining $\langle u^2 \rangle$. The lypholized trypsin powder S(Q) data (see Fig.13) did not show any D_2O peak as seen in the trypsin-D_2O solution (see Fig. 12).

FIG.11. S(Q) OF D2O AT T=300K

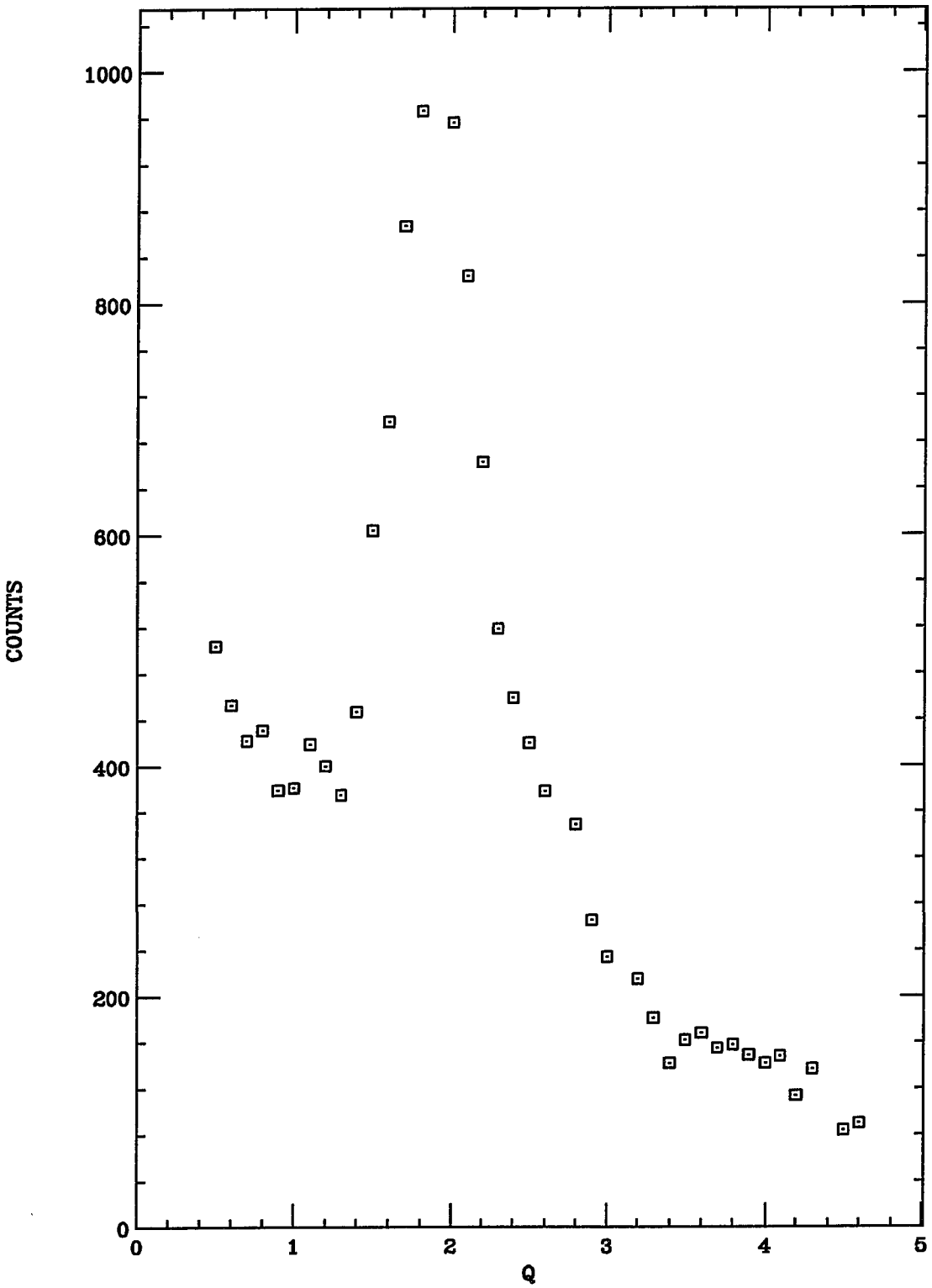

FIG.12. S(Q) OF TRYPSIN + D2O AT T=300K

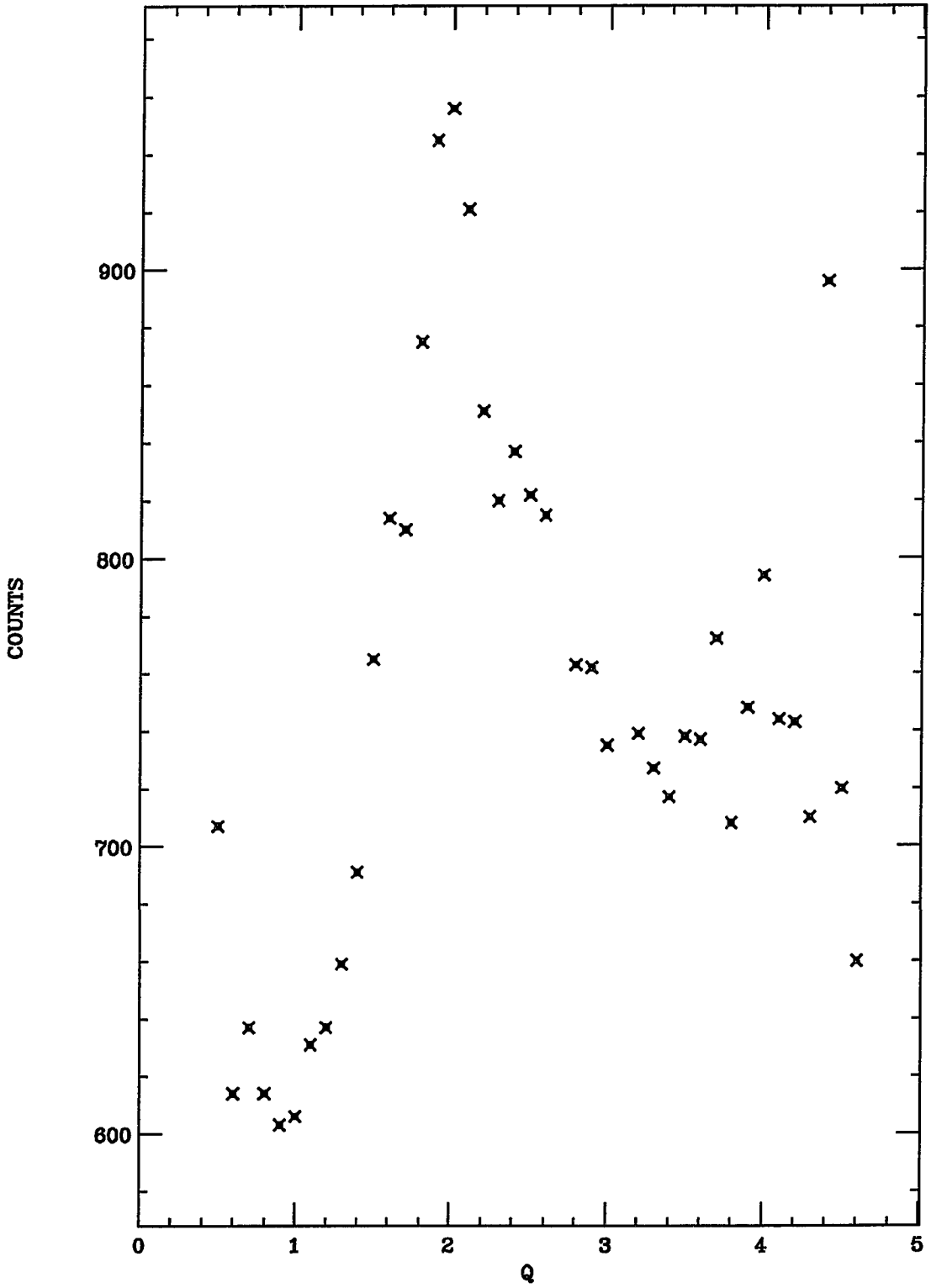

FIG.13. S(Q) OF POWDER TRYPSIN AT T=300K

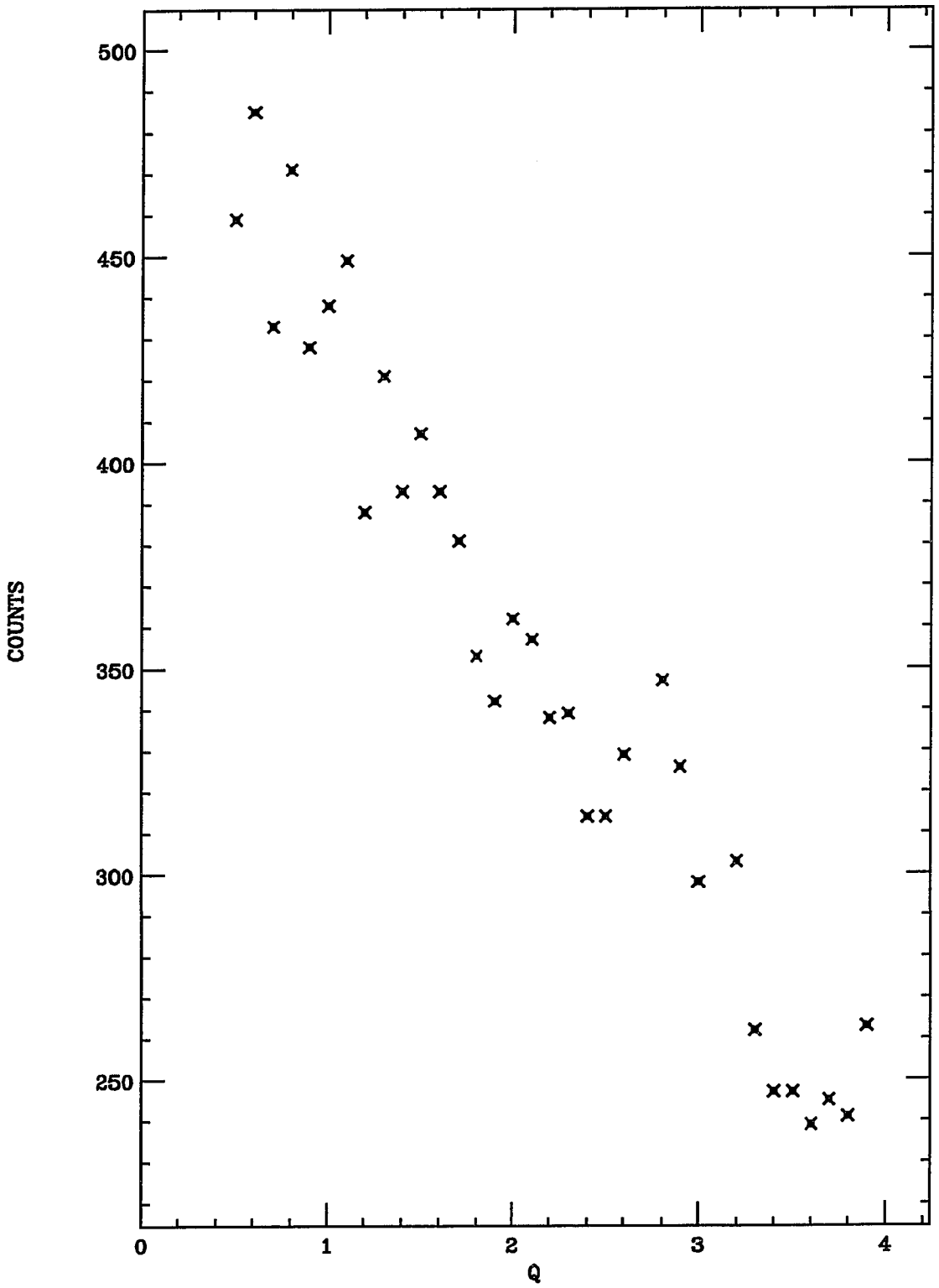

X. Conclusion and Future Study.

These preliminary studies have been very encouraging. The dynamics from the trypsin can be summed up as following:

– At small Q values, the trypsin hydrogens in liquid D_2O exhibit a large diffusive motion.

– Even though the evidence for the exact motional mechanism of these trypsin hydrogens is still inconclusive, these particles appear to have a jump-diffusion like behavior. According to the jump-diffusion model discussed in the text, the value of the diffusive coefficient D is significantly smaller than the value of D for pure water, and the residence time τ is larger than that of water.

– At T=300K, the Debye-Waller factor, which reveals the local high-frequency vibrational-amplitude, is larger than previous studies, and is in agreement with a recent molecular dynamics study of Garcia on crambin, a smaller protein. In previous studies as well as this study, the integrated intensities generally have shown a poor agreement with the DW factor.

– Comparision between solution, powder, and frozen trypsin motion indicate that the diffusive motion is greatly reduced in the powder and frozen solutions – the line-width becomes much narrower in powder and frozen trypsin.

Based on this preliminary study and recent trends in protein dynamics, our plan for future experiments is following. First, we would like to verify the leveling off of the line-width at high Q, since our present data showing the asymptotic behavior at one value, $Q^2 = 6.25$ Å^{-2}. More data at high Q will allow us to make a better analysis of the jump-length distribution function. With more data, it may be possible to determine the jump-length distribution $\rho(\mathbf{r})$ by Fourier-transform methods (refer to jump-diffusion theory section), which has not been done before (see appendix C).

Further experiments, with better statistics, will allow us to study the poor agreement of the measured integrated intensity with the Debye-Waller factor. This study is important because at present it is the one parameter that can be compared directly with molecular dynamics calculations and X-ray diffraction measurements, since there are few studies on the microscopic details of the diffusive motion.

The S(Q) measurements still need detailed study. It is possible that the D_2O peak in the solution data at ~ 2 $Å^{-1}$ might have different characteristics than in pure D_2O. This could reveal some properties of the interaction between protein and the solvent.

Our next stage of study will also include trypsin crystals. One recent trend of thought is that the motion of proteins can be studied by examining protein crystals, since proteins in crystalline form contain as much as 60% water molecules. Using the QNS method, we will be able to examine the dynamics of both solution and crystalline forms. The idea that the protein configuration makes transitions between many conformational substates is worth investigating in greater detail. We believe that QNS can provide a way to test this idea (see appendix C).

References.

1. McCammon JA, Harvey SC. (1987). *Dynamics of Proteins and Nucleic Acids.* Cambridge University Press, Cambridge. 1-2.

2. Frauenfelder H, Chu K, Philipp R. (1991). Physics from Proteins. In: *Biologically Inspired Physics.* Edited by L. Peliti. Plenum Press, NY. pp. 1-14.

3. van Gunsteren WF, Berendsen HJC. (1985). Molecular Dynamics Simulations: Techniques and Applications to Proteins. In: *Molecular Dynamics and Protein Structure.* Edited by J. Hermans. UNC Printing Department, NC. pp. 5-14.

4. Flores TP, Moss DS. (1991). Simulating the Dynamics of Macromolecules. In: *Molecular Dynamics Applications in Molecular Biology.* Edited by J. A. Goodfellow. MacMillian Press, UK. pp. 1-21.

5. Karplus M. (1984). Dynamics of Proteins. *Adv. Biophys.* 18, 165-190.

6. Smith JC. (1991). Protein Dynamics: Comparison of Simulations with Inelastic Neutron Scattering Experiments. *Quart. Rev. Biophys.* 24, 227-291.

7. Garcia AE. (1992). Large-Amplitude Nonlinear Motions in Proteins. *Phys. Rev. Lett.* 68, 2696-2699.

8. Bearden DW. (1986, unpublished). *A Quasi-Elastic Neutron Scattering Study of Hydrogen Dynamics in Aqueous Polymer Solutions.* Ph. D. Thesis. Physics Dept., Rice Univ. Houston, TX. 77251.

9. Lin C. *Macromolecular Dynamics Studied by Magnetic Resonance and Neutron Scattering*. Ph. D. Thesis. Physics Dept., Rice Univ. Houston. TX. 77251.

10. Stroud RM, Kay LM, Dickerson RE. (1972). The Crystal and Molecular Structure of DIP Inhibited Bovine Trypsin at 2.7 Å Resolution. In: *Cold Spring Harbor Symposia on Quantitative Biology*. Vol. XXXVI, 125-140.

11. Baker EN, Hubbard RE. (1984). Hydrogen Bonding in Globular Proteins. *Prog. Biophys. Molec. Biol.* 44, 97-179.

12. Stroud RM, Kay LM, Dickerson RE. (1974). The Structure of Bovine Trypsin: Electron Density Maps of the Inhibited Enzyme at 5 Å and at 2.7 Å Resolution. *J. Mol. Biol.* 83, 165-208.

13. Kossiakoff AA. (1984). Use of the Neutron Diffraction – H/D Exchange Technique to Determine the Conformational Dynamics of Trypsin. In: *Neutrons in Biology*. Plenum Press, New York, NY., pp. 281-304.

14. Bee M. (1988). *Quasielastic Neutron Scattering: Principles and Applications in Solid State, Chemistry, Biology and Materials Science.* Adam Hilger, UK. 9-10.

15. Lomer WM, Low GG. (1965). Introductory Theory. In: *Thermal Neutron Scattering.* Edited by P. A. Egelstaff. Academic Press, London. 10-50.

16. Squires GL. (1978). *Introductory to the Theory of Thermal Neutron Scattering.* Cambridge University Press, Cambridge.

17. Middendorf HD. (1984). Biophysical Applications of Quasi-elastic and Inelastic Neutron Scattering. *Ann. Rev. Biophys. Bioeng.* 13, 425-451.

18. Marshall W, Lovesey SW. (1971). *Theory of Thermal Neutron Scattering*. Oxford University Press, Oxford.

19. Volino F. (1978). Spectroscopic Methods for the Study of Local Dynamics in Polyatomic Fluids. In: *Microscopic Structure and Dynamics of Liquids*. Edited by J. Dupuy and A. J. Dianoux. Plenum Press, New York. 221-300.

20. Bee M. (1988). *Quasielastic Neutron Scattering: Principles and Applications in Solid State, Chemistry, Biology and Materials Science*. Adam Hilger, UK. 9-16; 66-71.

21. Springer T. (1972). *Quasielastic Neutron Scattering for the Investigation of Diffusive Motions in Solids and Liquids*. Springer-Verlag, Berlin. 30-35.

22. Lovesey S. (1984). *Theory of Neutron Scattering from Condensed Matter*. Claredon Press, Oxford. 1, 5-33; 59-73.

23. Middendorf HD. (1984). Biophysical Applications of Quasielastic and Inelastic Neutron Scattering. *Ann. Rev. Biophys. Bioeng.* 13, 425-451.

24. Smith JC. (1991). Protein Dynamics: Comparison of Simulations with Inelastic Neutron Scattering Experiments. *Quart. Rev. Biophys.* 24, 227-291.

25. Cusack S. (1982). Low Frequency Dynamics of Proteins Studied by Inelastic Neutron Scattering. In: *The Enzyme Catalysis Process*. Edited by A. Cooper and others. Plenum Press, New York. 103-122.

26. Giordano R, Salvato G, Wanderlingh F, Wanderlingh U. (1990). Quasielastic and Inelastic Neutron Scattering in Macromolecular Solutions. *Phys. Rev.* A41, 689-696.

27. Springer T. (1972). *Quasielastic Neutron Scattering for the Investigation of Diffusive Motions in Solids and Liquids*. Springer-Verlag, Berlin. 62-69.

28. Egelstaff PA. (1967). *An Introduction to the Liquid State*. Academic Press, London. 118-132.

29. Bee M. (1988). *Quasielastic Neutron Scattering: Principles and Applications in Solid State, Chemistry, Biology and Materials Science*. Adam Hilger, UK. 107-147.

30. Trantham EC. (1981). *Diffusive Motion of Water in Biological and Model Systems*. Ph. D. Thesis. Physics Dept., Rice Univ., Houston, TX. 77251.

31. Middendorf HD, Randall JJ, Crespi HL. Neutron Spectroscopy of Hydrogenous and Biosynthetically Deuterated Proteins. In: *Neutrons in Biology*. Edited by P. B. Schoenborn. Plenum Press, New York, NY., pp. 381-400.

32. Moore PB. (1982). Small-Angle Scattering Techniques for the Study of Biological Macromolecules and Macromolecular Aggregates. In: *Methods of Experimental Physics*. Vol. 20. Edited by G. Ehrenstein and H. Lecar. Academic Press, NY, pp. 337-389.

33. Hutchings MT, Lowde RD, Tindle GL. (1991). The Determination of $S(Q,\omega)$ from Triple-Axis Spectrometer Data. *Inst. Phys. Conf. Ser.* No. 81, chapter 5.

34. Chesser NJ, Axe JD. (1973). Derivation and Experimental Verification of Normalized Resolution Function for Inelastic Neutron Scattering. *Acta Cryst.* A29, 160-169.

35. Cooper MJ, Nathans R. (1967). The Resolution Function in Neutron Diffractometry I. The Resolution Function of a Neutron Diffractometer and Its Application to Phonon Measurements. *Acta Cryst.* 23, 375-67.

36. S. Shapiro (1992). Private communication.

37. Wertheim GK, Butler MA, West RW, Buchanan DNE. (1974). Determination of Gaussian and Lorentzian Content of Experimental Line Shapes. *Rev. Sci. Instr.* Vol. 45, 11.

38. Kielkofp JF. (1973). New Approximation to the Voigt Function with Applications to Spectral-Line Profile Analysis. *J. Opt. Socei. of Amer.* 63, 987-995.

39. Bakshi V, Kearney RJ. (1989). New Tables of the Voigt Function. *J. Quant. Spectrosc. Radiat. Transfer.* 42, 111-115.

40. Flores-Llamas, Cabral-Prieto AC, Jimenez-Domiguez HJ, Bravo-Ortega AB. (1990). Tables of the Voigt Profile with Ten Digits. *Nucl. Inst. and Meth. in Phys. Res.* A287, 557-558.

41. *Handbook of Mathematical Functions*. (1964). Edited by M. Abramowitz, I. A. Stegun. National Bureau of Standards Applied Mathematics Series. 55, 297-304.

42. Trantham EC. (1979, unpublished). *Diffusive Motion of Water in Biological and Model Systems*. Master Thesis. Physics Dept., Rice Univ., Houston, TX. 77251.

43. Press WH, Flannery BP, Teukolsky SA, Vettliing WT. (1989). *Numerical Recipes* (Fortran). Cambridge University Press, Cambridge. 521-528.

44. Bee M. (1988). *Quasielastic Neutron Scattering: Principles and Applications in Solid State, Chemistry, Biology and Materials Science.* Adam Hilger, UK. 72-8.

45. BNL *Handbook on Reactors.* U. S. Government.

46. Hall PL, Ross DK. (1981). Incoherent Neutron Scattering Functions for Random Jump Diffusion in Bounded and Infinite Media. *Mol. Phys.* 673-82.

47. Rorschach HE. Private communication.

48. Bee M. (1988). *Quasielastic Neutron Scattering: Principles and Applications in Solid State, Chemistry, Biology and Materials Science.* Adam Hilger, UK. 167-175; 378-385.

49. Middendorf HD, Sir Randall J, FRS. (1980). Molecular Dynamics of Hydrated Proteins. *Phil. Trans. R. Soc. Lond.* B290, 639-655.

50. Brook III CL, Karplus M. (1989). Solvent Effects on Protein Motion and Protein Effects on Solvent Motion. *J. Mol. Biol.* 208, 159-181.

51. Teixeira J, Bellissent-Funel MC, Chen SH, Dianoux AJ. (1985). Experimental Determination of the Nature of Diffusive Motions of Water Molecules at Low Temperature. *Phys. Rev.* A31, 1913-1917.

52. Rorschach HE, Bearden DW, Hazlewood CF, Heidorn DB, Nicklow RM. Quasi-elastic Scattering Studies of Water Diffusion. *Scanning Microscopy*. Vol. 1. 4, 2043-2049.

53. Frauenfelder H, Petsko GA, Tsernoglou D. (1979). Temperature-dependent X-ray Diffraction as a Probe of Protein Structural Dynamics. *Nature*. 280, 558-563.

54. Wong CF, McCammon JA. (1987). Computer Simulation and the Design of New Biological Molecules. *Israel J. of Chem.* 27, 211-15.

Appendix A.

A. *Quantum Mechanical Formulation of Neutron Scattering Function.*

An elegant technique for neutron spectroscopic experiments was given by Volino (1978) in terms of the coupling between the two systems, in our case, the neutron and the sample.<19>

We assume the system, in this case the protein sample, is in thermal equilibrium at temperature T. The sample consists of N particles (or units) and is represented by its Hamiltonian, H_S, with eigenstates $|m'\rangle$ and eigevalues $E_{m'}$. The probability that the sample occupies state $|m'\rangle$ is

$$P_{m'} = \frac{1}{Z_S} \exp(-\beta E_{m'}) \qquad \text{(A-1)}$$

with $\beta=(k_bT)^{-1}$, k_b being the Boltzmann constant, and $Z_S = \sum_{i=1}^{m} \exp(-\beta E_{m'})$. (A-2)

The second system is the neutron. The neutron is characterized by its Hamiltonian, H_n, with the corresponding eigenstates $|m\rangle$ and eigenvalues E_m. The neutron interacts with the sample through the coupling Hamiltonian H_c. The basic principle is as follows: first, the neutron is assumed to be in a defined dynamical state $|m\rangle$. This means that the neutrons are well collimated and monochromatized. As the coupling is turned on, the neutron state varies with time to another state $|n\rangle$. The sample, initially at the state $|m'\rangle$, is also changed to another state $|n'\rangle$. In this neutron-sample interaction, we assume that H_c is small compared to H_S and H_n . Using the Fermi Golden Rule, we have:

$$W_{nn'\,mm'} = \frac{2\pi}{\hbar} |\langle n'| \langle n| H_c |m\rangle |m'\rangle|^2 \, \delta(E_m+E_{m'}-E_n-E_{n'}) \qquad \text{(A-3)}$$

$W_{nn'\,mm'}$ denotes the probability per unit time that the total system, the sample and the neutron, changes from $|m\rangle|m'\rangle$ to $|n\rangle|n'\rangle$.

The aim of spectroscopic experiments is to measure a quantity which is proportional to W_{nm}, as a function of $|n\rangle$ or $|m\rangle$. Dynamical information on the sample is obtained, since W_{nm} is a function of variables in the sample. The problem is therefore to focus on calculating W_{nm} and to relate it to measurable quantities. The probability per unit time that gives the change of the state of the neutron is given by,

$$W_{nm} = \sum_{n'm'} W_{nn'\,mm'}\, P_{m'} \tag{A-4}$$

$$= \frac{1}{Z_s} \sum_{n'm'} W_{nn'\,mm'} \exp(-\beta E_{m'}) \tag{A-5}$$

For convenience, we define $\overline{H_c}$, the average of H_c between the initial and final states of the sample:

$$\overline{H_c} = \langle n|\, H_c\, |m\rangle. \tag{A-6}$$

$\overline{H_c}$ only depends on the state of the sample. We now can rewritten Eq. (A-5) as the following:

$$W_{nm} = \frac{2\pi}{\hbar}\, \frac{1}{Z_s} \sum_{n'm'} \exp(-\beta E_{m'})\; |\langle n'|\, \overline{H_c}\, |m'\rangle|^2\, \delta(E_m + E_{m'} - E_n - E_{n'}) \tag{A-7}$$

with $\hbar\omega = E_m - E_n$ = energy gain of the neutron,

$\hbar\omega_{n'm'} = E_{n'} - E_{m'}$ = energy loss of the sample.

Eq. (A-7) now becomes

$$W_{nm} = \frac{2\pi}{\hbar}\frac{1}{Z_s}\sum_{n'm'}\exp(-\beta E_{m'})\ |\langle n'|\ \overline{H_c}\ |m'\rangle|^2\ \delta(\omega_{n'm'} - \omega) \qquad \text{(A-8)}$$

The delta function ensures an adequate expression for discrete peaks of the spectrum, for a purely quantum mechanical system. In order to describe other complicated systems, it is advantageous to formulate an equivalent expression for W_{nm}. This can be obtained by noting the hermiticity of H_c and the integral representation for the δ function. We have

$$|\langle n'|\ \overline{H_c}\ |m'\rangle|^2 = \langle n'|\ \overline{H_c}\ \ |m'\rangle\langle m'|\ \overline{H_c}^{+}|n'\rangle \qquad \text{(A-9a)}$$

and

$$\delta(\omega_{n'm'} - \omega) = \frac{1}{2\pi}\int_{-\infty}^{\infty} dt\ \exp\ i(\omega_{n'm'} - \omega)t \qquad \text{(A-9b)}$$

Substituting (A-9a),(A-9b) into (A-8), we obtain

$$W_{nm} = \frac{2\pi}{\hbar^2}\frac{1}{Z_s}\sum_{n'm'}\int_{-\infty}^{\infty} dt\ \exp\ i(\omega_{n'm'} - \omega)t\ \ x$$

$$\exp(-\beta E_{m'})\ \langle m'|\ \overline{H_c}\ |n'\rangle\langle n'|\ \overline{H_c}^{+}|m'\rangle \qquad \text{(A-10)},$$

$$= \frac{2\pi}{\hbar^2}\frac{1}{Z_s}\sum_{n'm}\int_{-\infty}^{\infty} dt\ \exp\ (-i\omega t)$$

$$\exp(-\beta E_{m'})\ \langle m'|\ \overline{H_c}\ |n'\rangle\langle n'|\exp(-i\frac{E_{n't}}{\hbar})\ \overline{H_c}^{+}\exp(i\frac{E_{m't}}{\hbar})|m'\rangle\ . \qquad \text{(A-11)}$$

The double sum denotes the expression of a trace in the Hilbert space of the sample states, and

$$W_{nm} = \frac{1}{\hbar^2} \int_{-\infty}^{\infty} dt \exp(-i\omega t)\, \mathrm{Tr}\, \{\hat{\rho}_S\, \overline{H_C}^{+}(0)\, \overline{H_C}(t)\} \qquad \text{(A-12)}$$

where, $\hat{\rho}_S$ is the equilibrium density matrix of the sample

$$\hat{\rho}_S = \frac{1}{Z_S} \exp(-\beta H_S)\,, \qquad \text{(A-13)}$$

and $\overline{H_C}(t)$ is the Heisenberg representation of the operator $\overline{H_C} = \overline{H_C}(0)$,

$$\overline{H_C}(t) = \exp\left(-\frac{i}{\hbar} H_S t\right) \overline{H_C} \exp\left(\frac{i}{\hbar} H_S t\right). \qquad \text{(A-14)}$$

The expresion

$$\mathrm{Tr}\, \{\hat{\rho}_S\, \overline{H_C}^{+}(0)\, \overline{H_C}(t)\} = \langle \overline{H_C}^{+}(0)\, \overline{H_C}(t) \rangle \equiv C_{\overline{H_C}\ \overline{H_C}}(t) \qquad \text{(A-15)}$$

is the quantum mechanical self-correlation of $\overline{H_C}$. If the system is classical, then $\overline{H_C}$ is a classical function of the variables in the sample space and $C_{\overline{H_C}\ \overline{H_C}}(t)$ is replaced by its classical equivalent. Finally, the probability of the transition W_{nm} is obtained in term of the time Fourier-transform of $C_{\overline{H_C}\ \overline{H_C}}(t)$,

$$C_{\overline{H_C}\ \overline{H_C}}(\omega) = \frac{1}{2\pi} \int_{-\infty}^{\infty} dt \exp(-i\omega t)\; C_{\overline{H_C}\ \overline{H_C}}(t) \qquad \text{(A-16)}$$

and

$$W_{nm} = \frac{2\pi}{\hbar^2}\; C_{\overline{H_C}\ \overline{H_C}}(\omega)\,. \qquad \text{(A-17)}$$

The inverse transition probability W_{mn} from state $|m\rangle$ to state $|n\rangle$ can be obtained by changing ω into $-\omega$. It can be easily shown, through conservation of energy, that

$$W_{nm} = \exp(-\beta\hbar\omega)\, W_{mn} \,. \qquad \text{(A-18)}$$

This means that the neutron lose and gain of energy are directly related to one another by a population factor exp ($-\beta\hbar\omega$). This shows a lack of symmetry in the probability per unit time of transition W_{nm} – representing the principle of detailed balance thru the differing values of the probability for the gain or loss of energy by the neutron.

Appendix B.

After completing major portions of this thesis, further QNS studies were done on trypsin. These experiments are a continuation of our studies of the motion of the protein trypsin. We have now completed more detailed studies on the scattering from a 20% trypsin solution in D_2O and trypsin single crystals.

The data for the solution exhibits a maximum in the line width at Q^2 near 4 $Å^{-2}$. This behavior is characteristic of a jump diffusion process with restricted jump lengths. A similar behavior has been observed for hydrogen diffusing in metals. We believe that the maximum in the line width is related to the rotational motion of the trypsin side chains during transitions between microconformational states. At present, we are still working on a theory to explain this motion.

The data for scattering from the crystals was obtained from a sample chamber containing a large number of small crystal (about 0.5 - 1 mm) that had been soaked in D_2O for approximately two weeks. The easily exchangeable protons would have been removed, so that we observe the scattering from the protons closely associated with the trypsin. The broadening in the crystal is greatly reduced from that in the solution. This is strong evidence against the idea that X-ray studies of protein motion in crystals can be used as indicative of the motion in solutions. A study done on myoglobin crystals also shows a similar behavior to that of trypsin crystals.

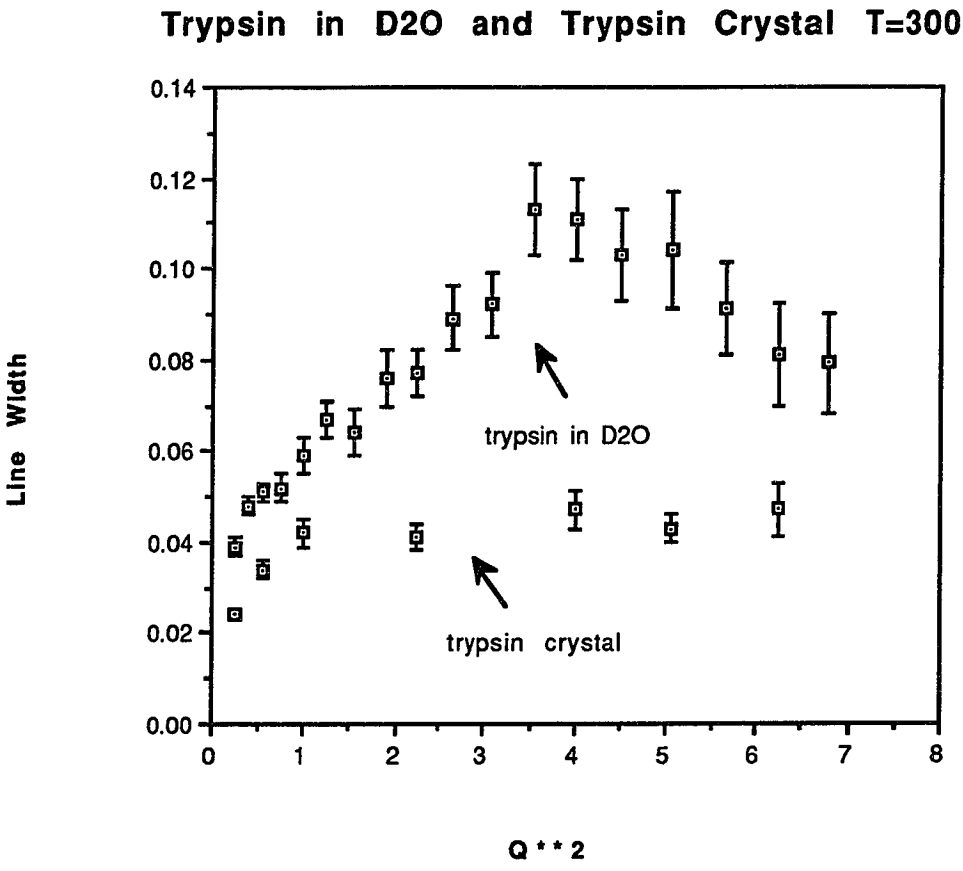
Trypsin in D2O and Trypsin Crystal T=300K
Line Width
0.14
0.12
0.10
0.08
0.06
0.04
0.02
0.00
0
1
2
3
4
5
6
7
8
trypsin in D2O
trypsin crystal
Q**2

Appendix C.

Quasi-elastic scattering studies were conducted on the dry powder, 20% trypsin-D_2O solutions, and pure D_2O as a function of temperature. The following scans were made:

a) 20% trypsin-D_2O solution: $S(Q,\omega)$ was measured for $0.5 < Q < 2.5$ Å^{-1} for T = 200, 280, 300 K. An S(Q) scan was made at 300 K for $0.5 < Q < 4.6$ Å^{-1}.

b) Powdered trypsin: $S(Q,\omega)$ was measured for $0.5 < Q < 2.5$ Å^{-1} at 300 K, and an S(Q) scan was made at 300 K for $0.5 < Q < 4.6$ Å^{-1}.

c) D_2O: $S(Q,\omega)$ and S(Q) were measured at 300 K for the above Q ranges.

d) The spectrometer resolution function was measured at fixed Q (= 1.5 Å^{-1}).

The data collected in constant-Q mode are plotted in the following pages. The fit data are shown without the error bars. The D_2O background is also included (these are the lower data points).

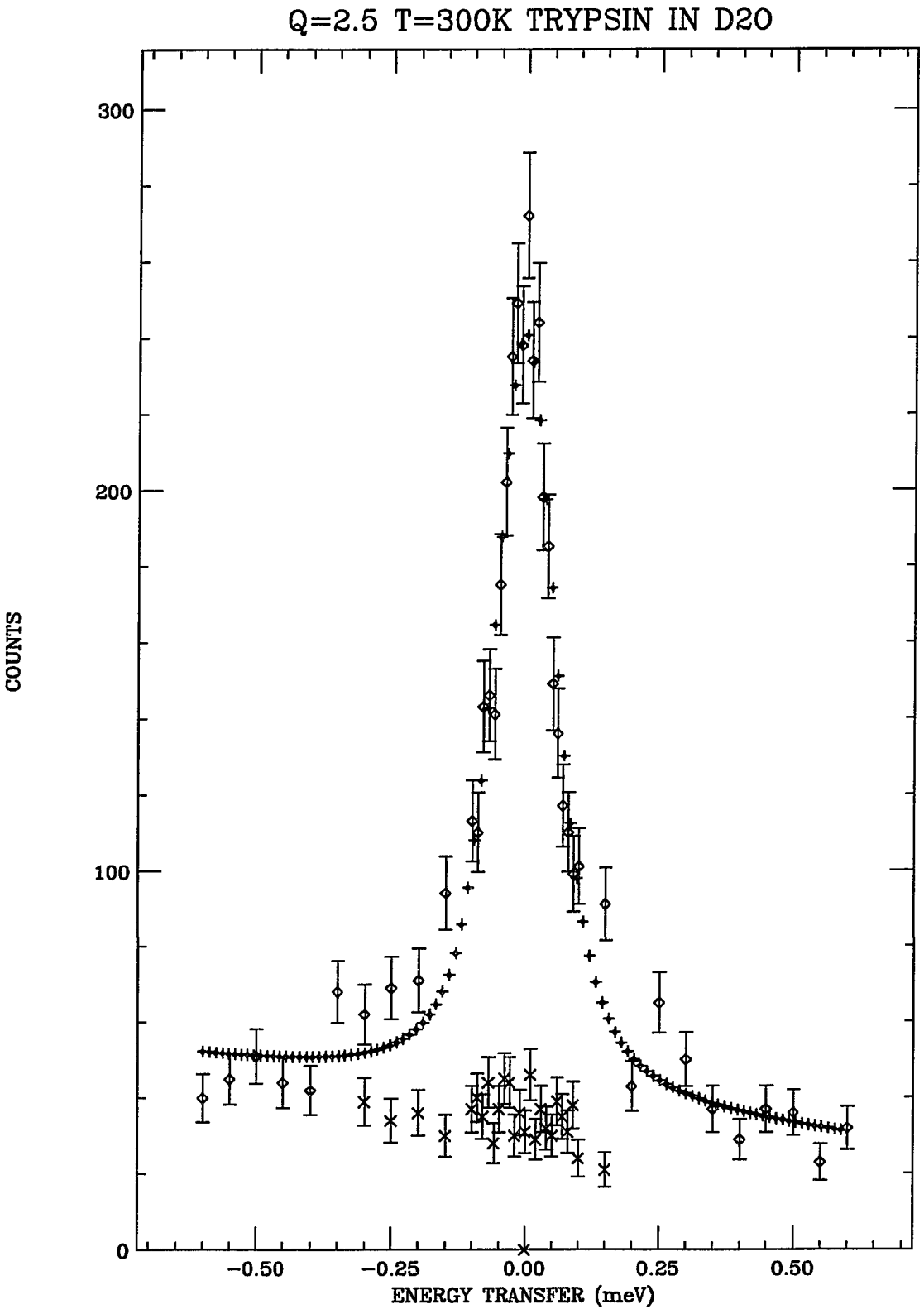
Q=2.5 T=300K TRYPSIN IN D2O
COUNTS
300
200
100
0
-0.50
-0.25
0.00
0.25
0.50
ENERGY TRANSFER (meV)

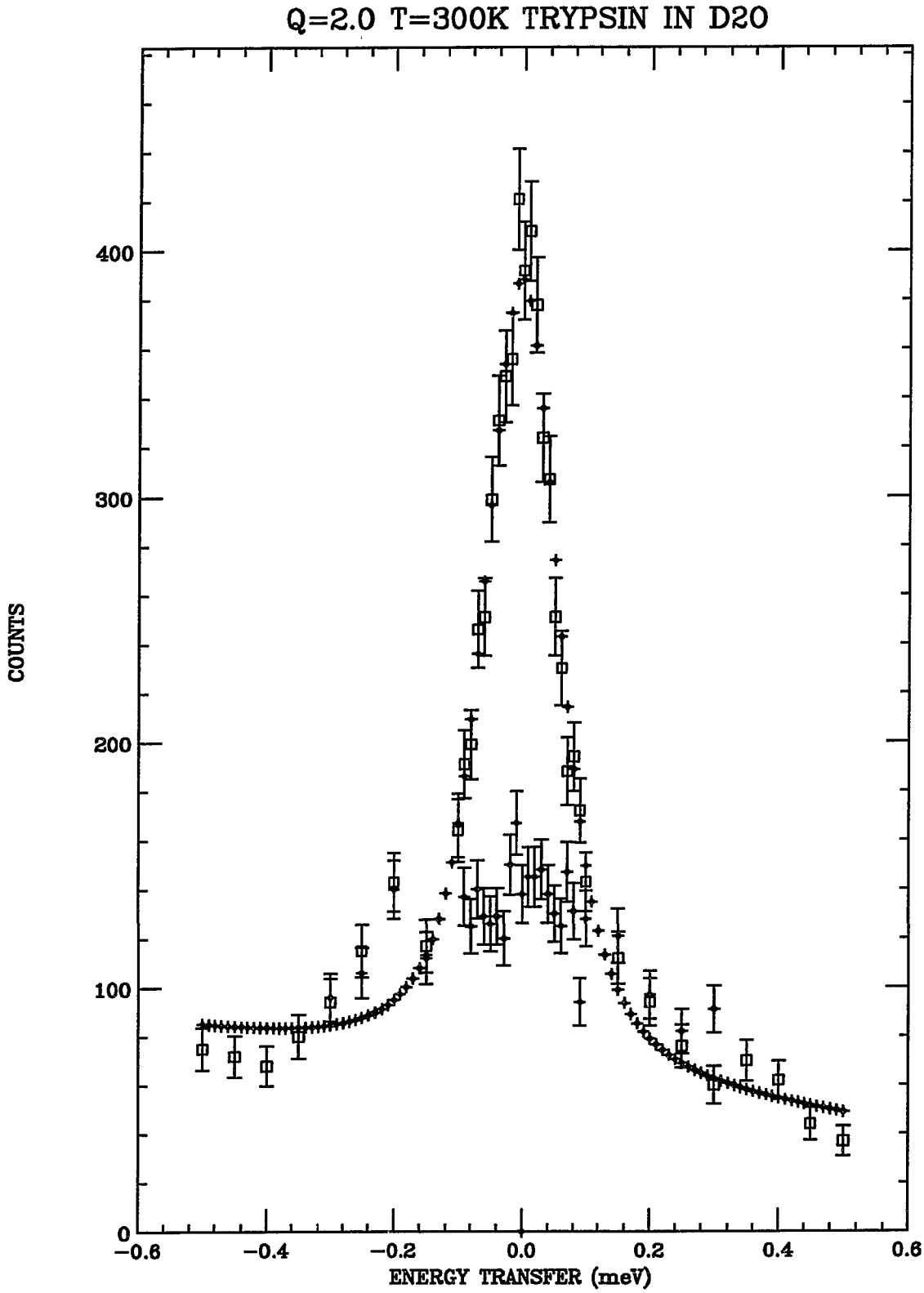
Q=2.0 T=300K TRYPSIN IN D2O
COUNTS
0
100
200
300
400
−0.6
−0.4
−0.2
0.0
0.2
0.4
0.6
ENERGY TRANSFER (meV)

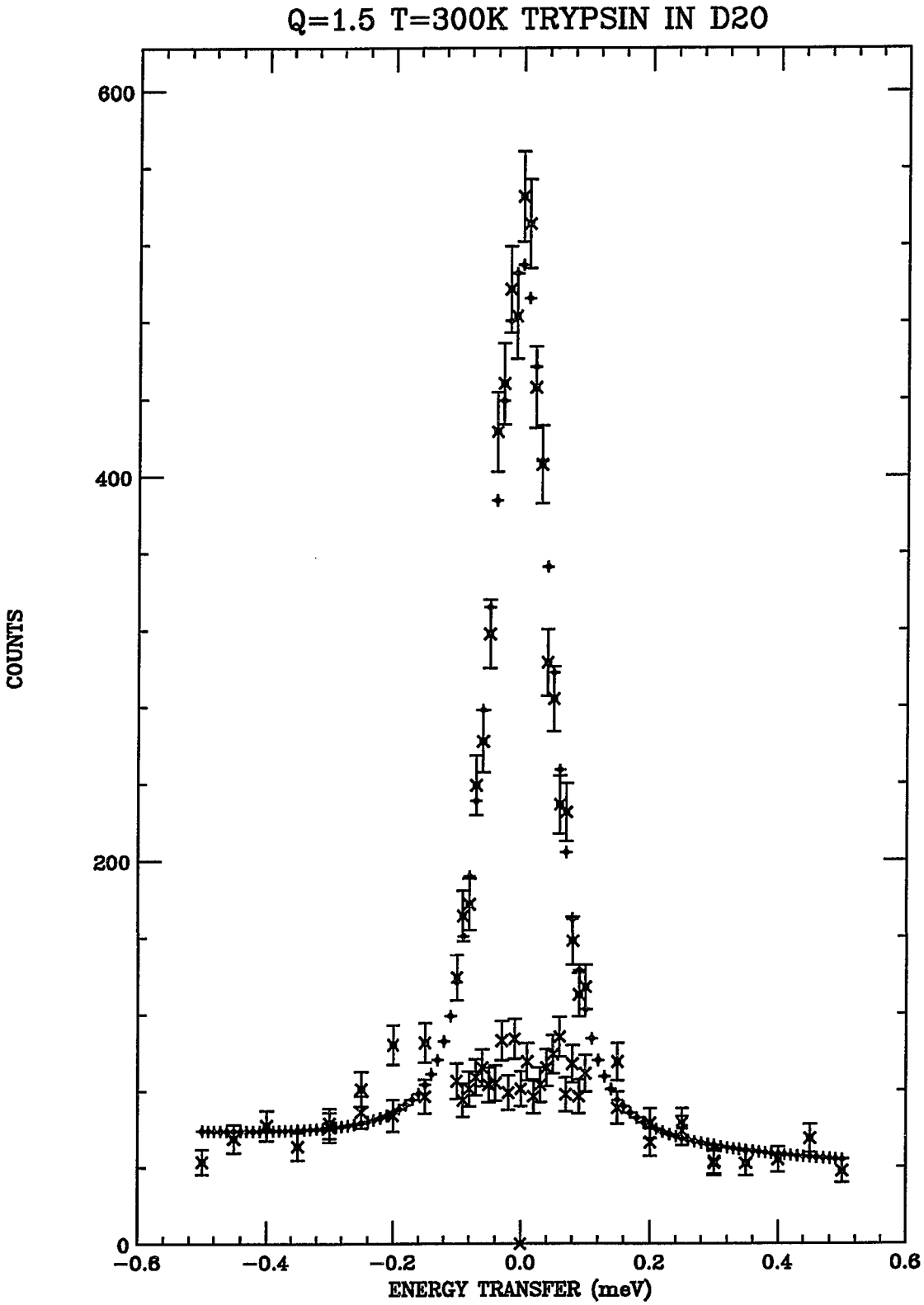
Q=1.5 T=300K TRYPSIN IN D20
COUNTS
600
400
200
0
−0.6
−0.4
−0.2
0.0
0.2
0.4
0.6
ENERGY TRANSFER (meV)

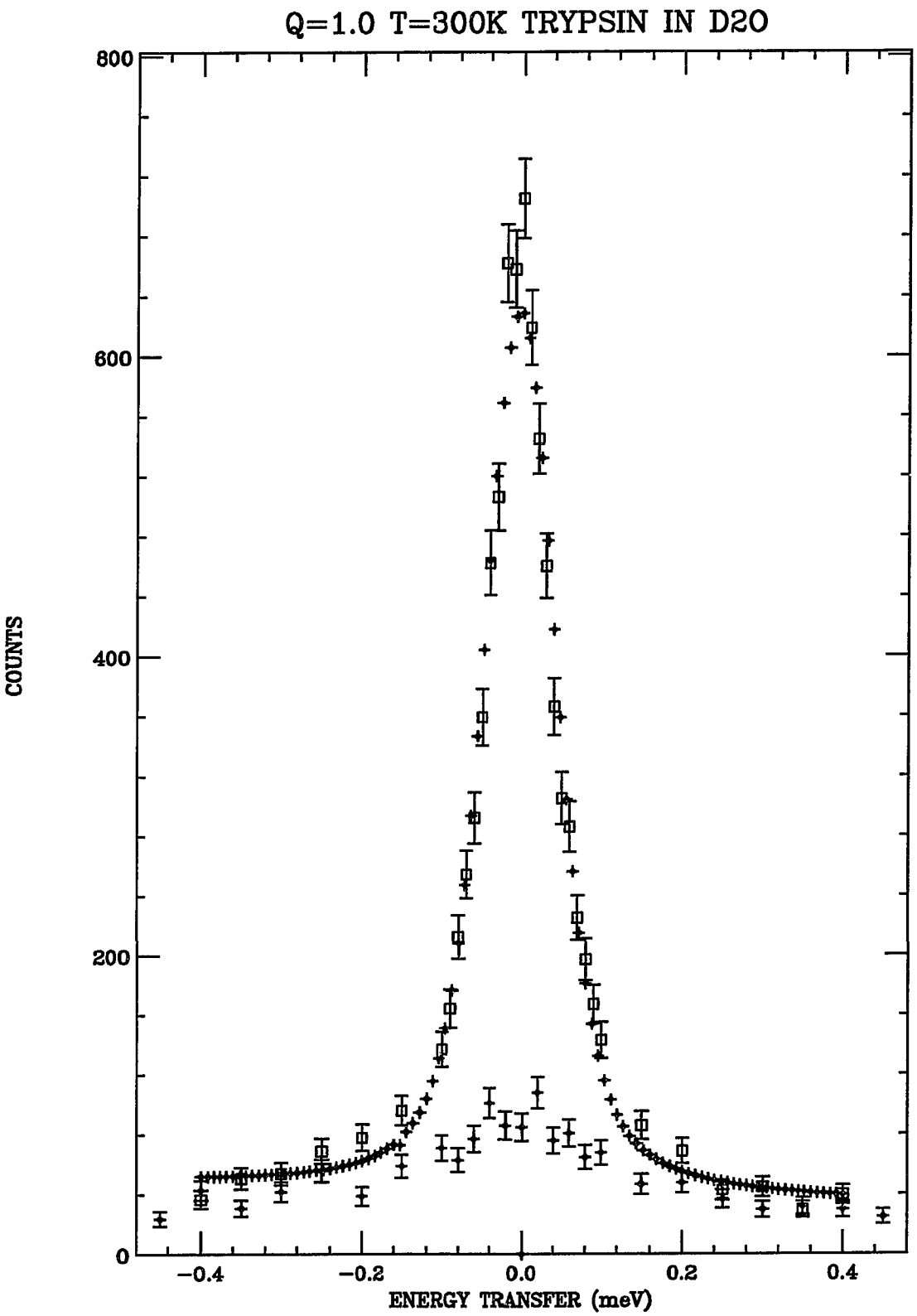
Q=1.0 T=300K TRYPSIN IN D2O
COUNTS
800
600
400
200
0
−0.4
−0.2
0.0
0.2
0.4
ENERGY TRANSFER (meV)

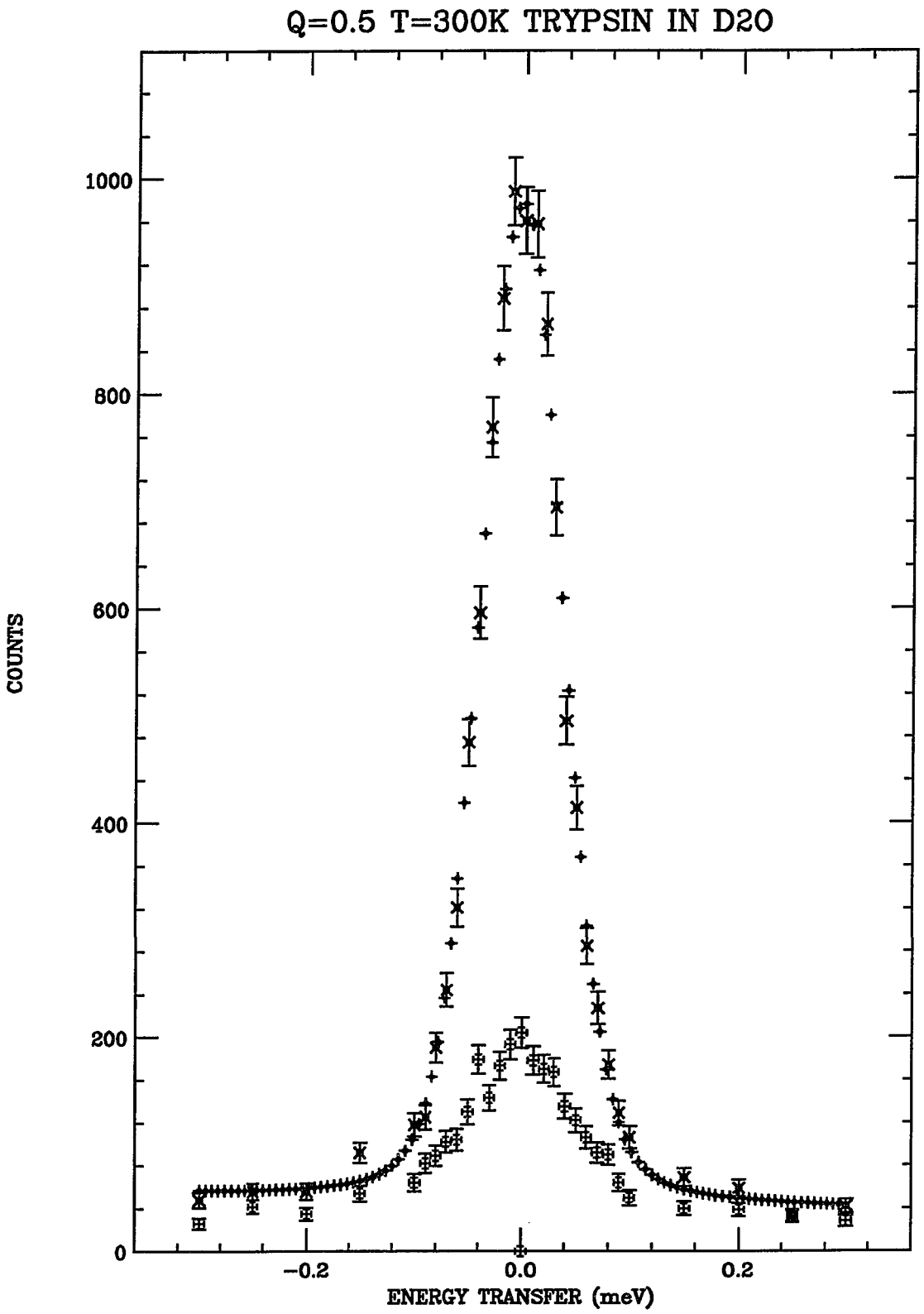
Q=0.5 T=300K TRYPSIN IN D20
COUNTS
1000
800
600
400
200
0
-0.2
0.0
0.2
ENERGY TRANSFER (meV)

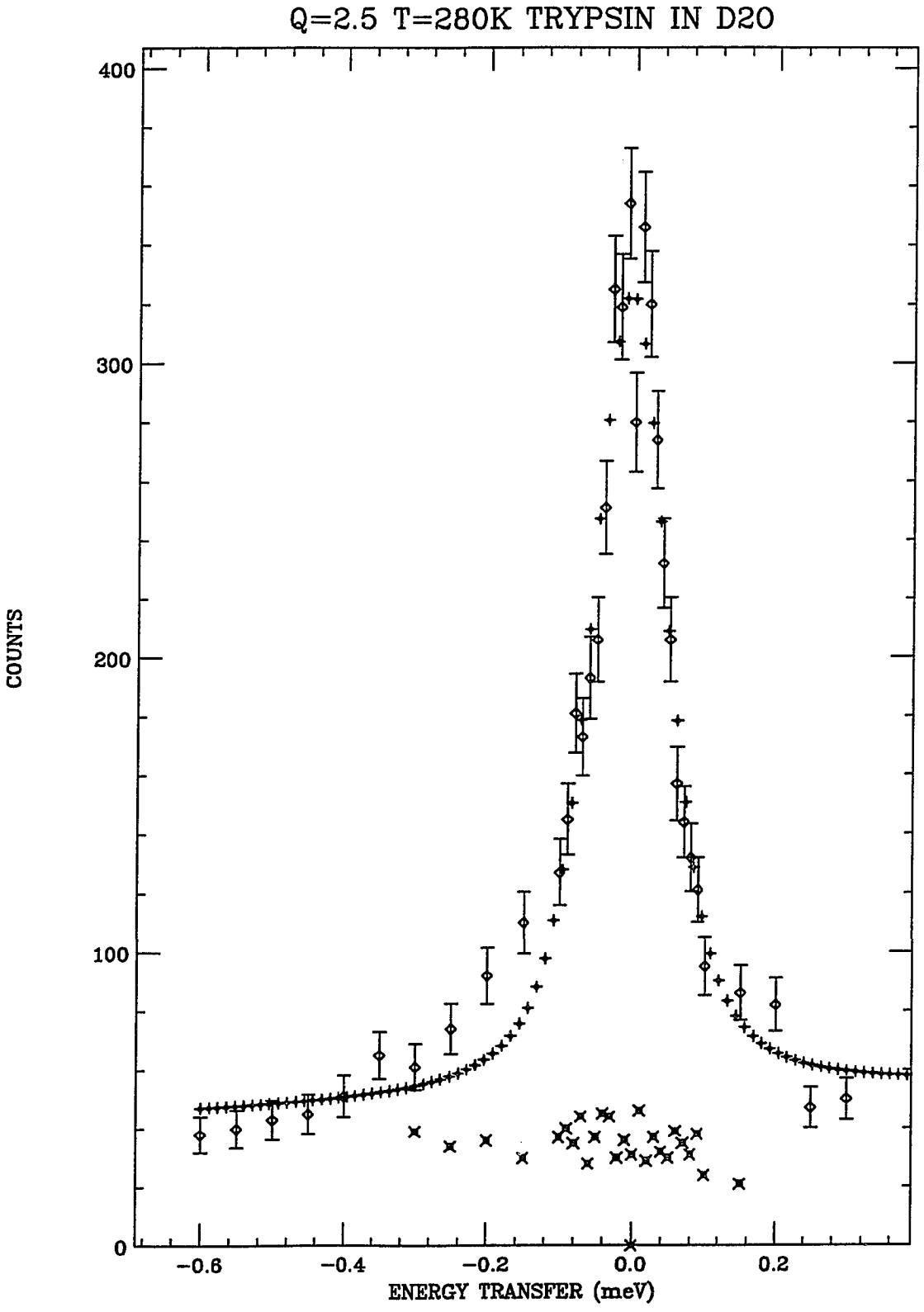
Q=2.5 T=280K TRYPSIN IN D2O
COUNTS
400
300
200
100
0
−0.6
−0.4
−0.2
0.0
0.2
ENERGY TRANSFER (meV)

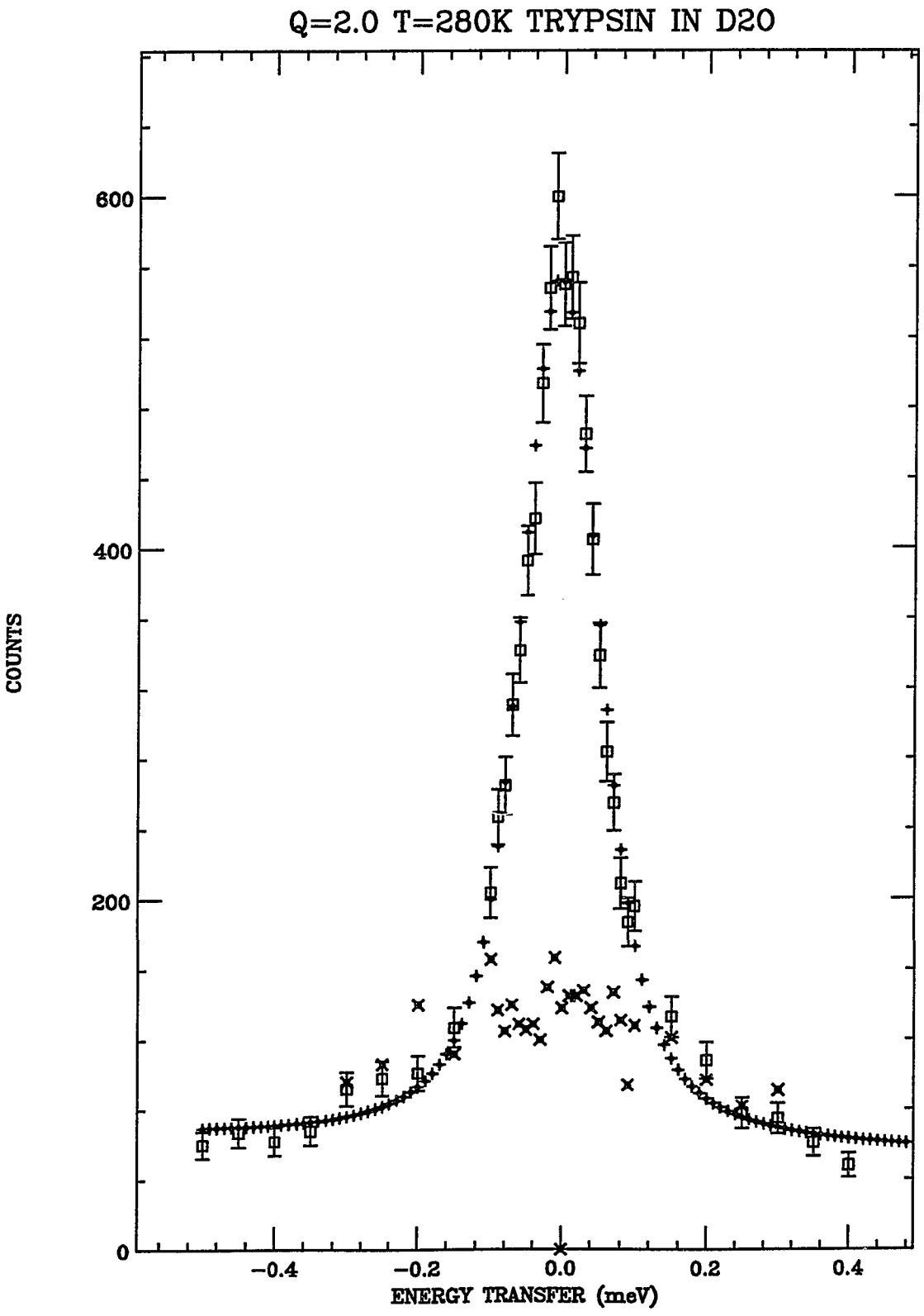
Q=2.0 T=280K TRYPSIN IN D20
COUNTS
600
400
200
0
−0.4
−0.2
0.0
0.2
0.4
ENERGY TRANSFER (meV)

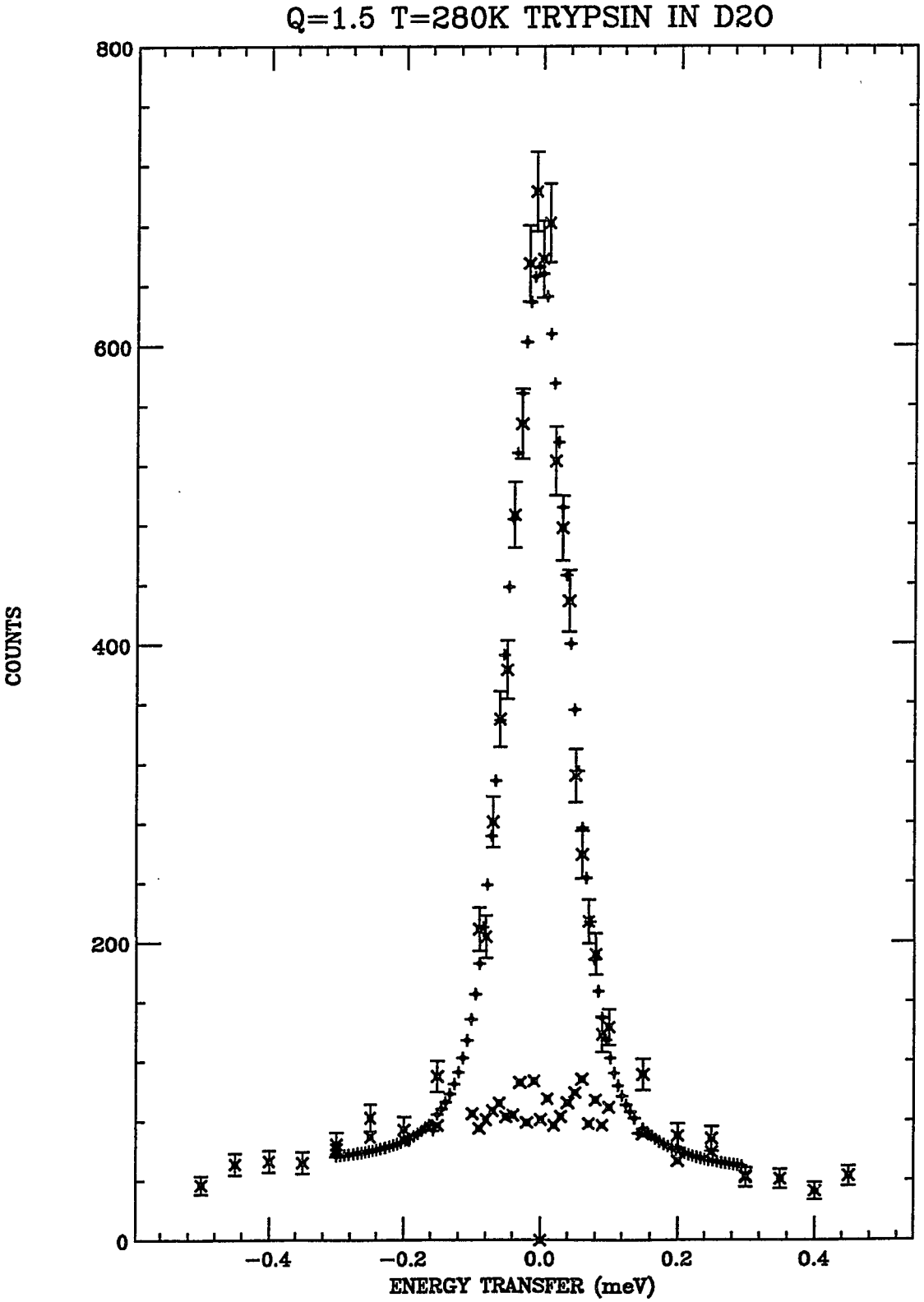
Q=1.5 T=280K TRYPSIN IN D2O
800
600
400
200
0
COUNTS
−0.4
−0.2
0.0
0.2
0.4
ENERGY TRANSFER (meV)

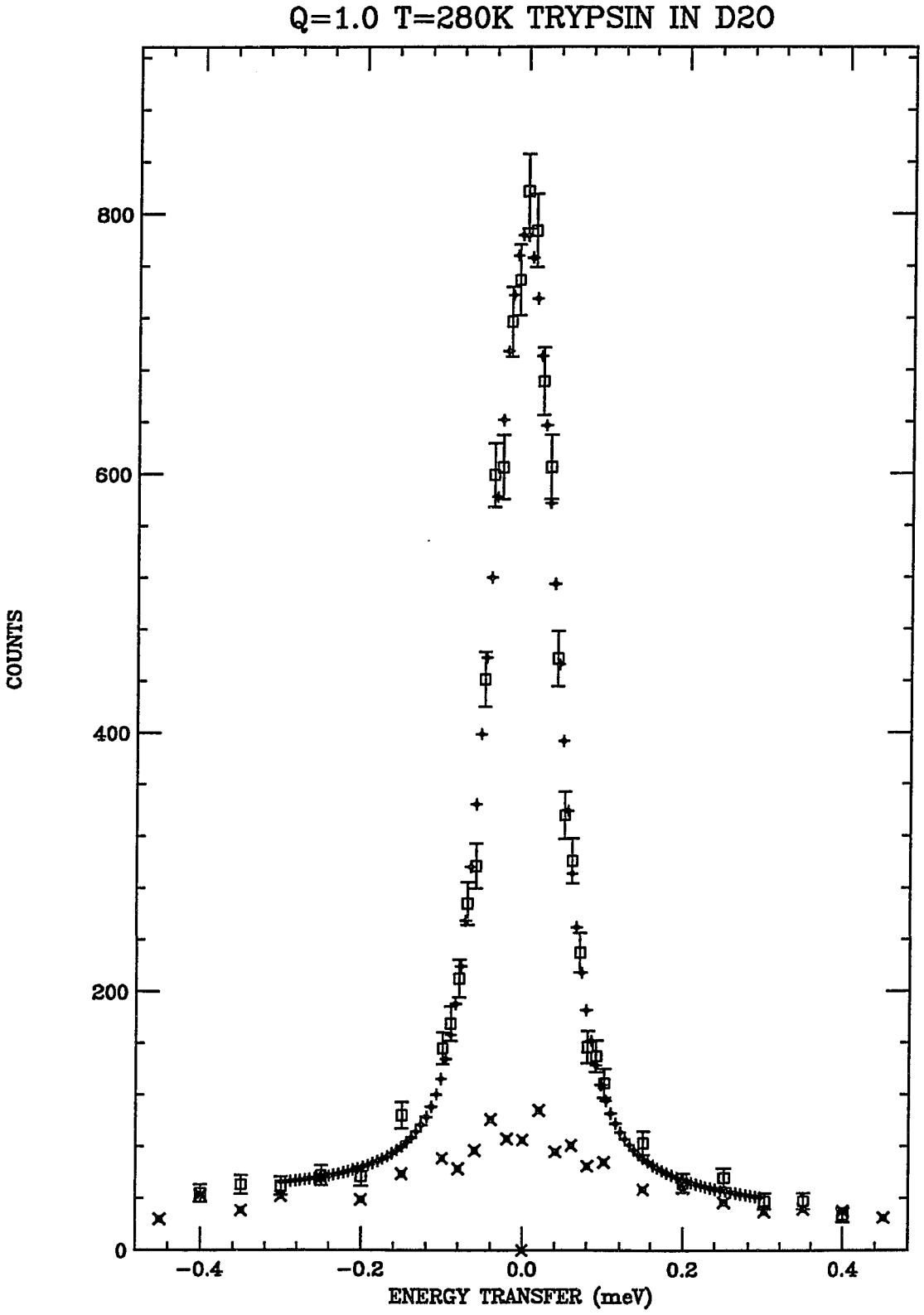
Q=1.0 T=280K TRYPSIN IN D20
COUNTS
800
600
400
200
0
−0.4
−0.2
0.0
0.2
0.4
ENERGY TRANSFER (meV)

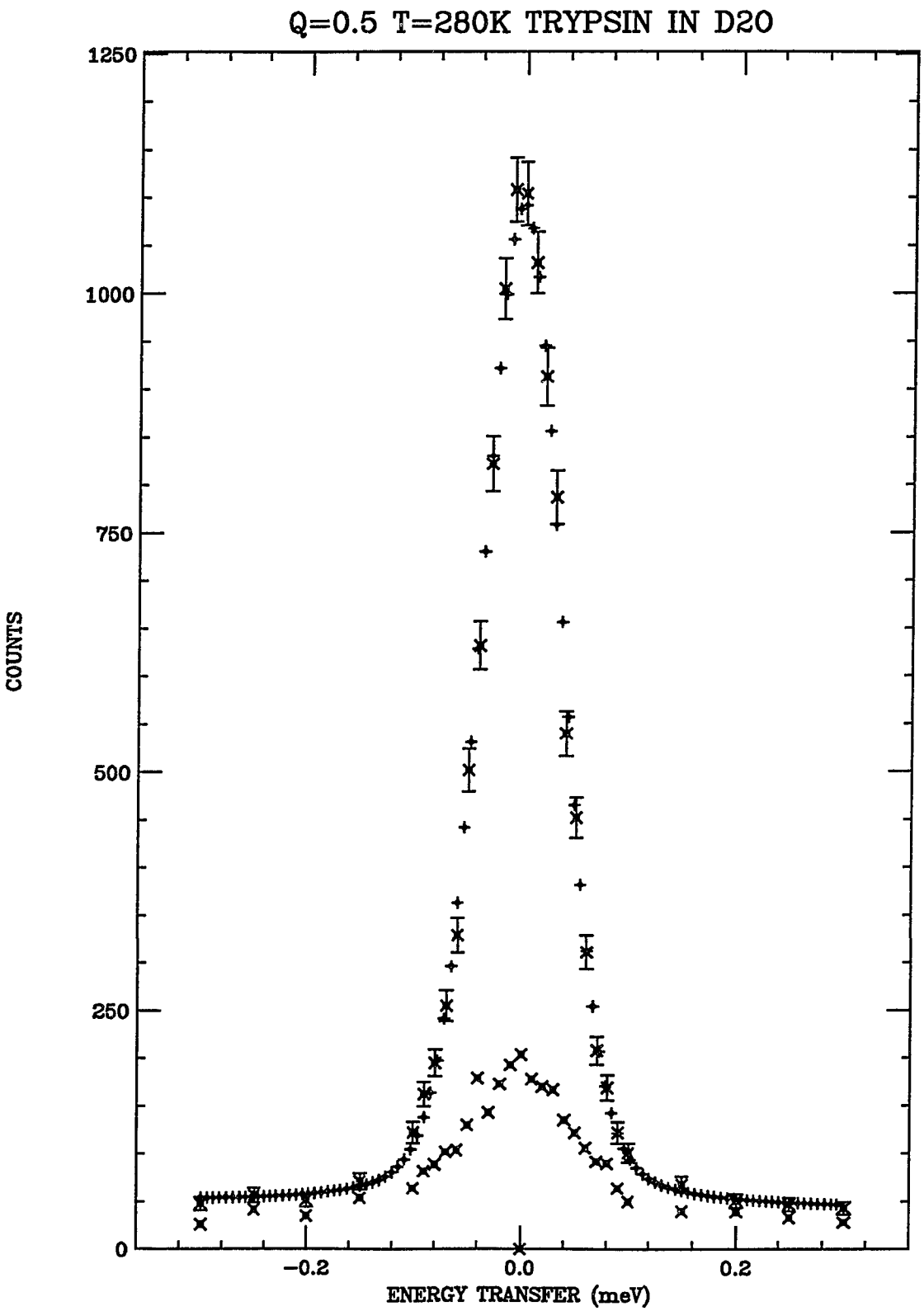
Q=0.5 T=280K TRYPSIN IN D2O
1250
1000
750
500
250
0
COUNTS
-0.2
0.0
0.2
ENERGY TRANSFER (meV)

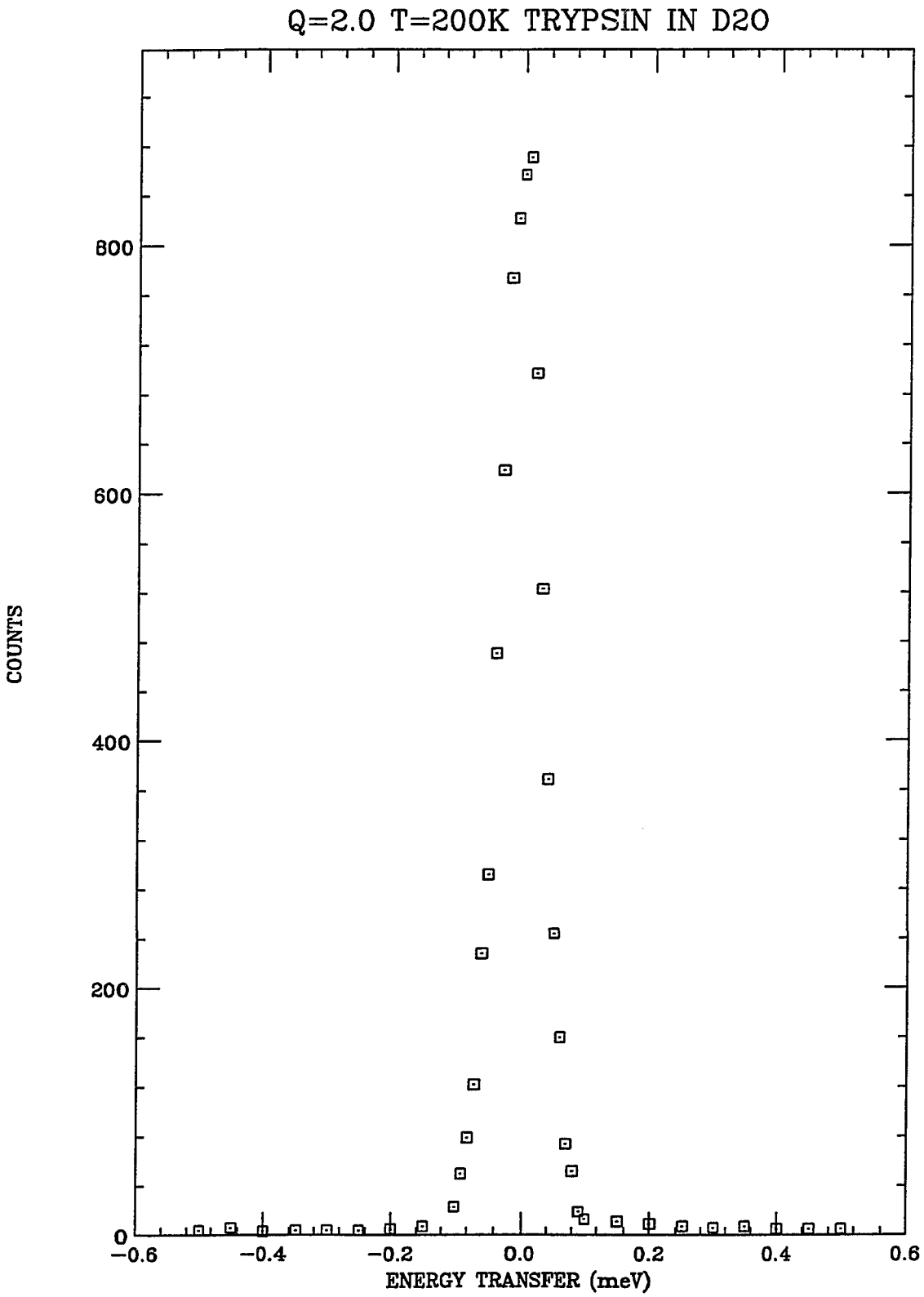
Q=2.0 T=200K TRYPSIN IN D2O
COUNTS
800
600
400
200
0
−0.6
−0.4
−0.2
0.0
0.2
0.4
0.6
ENERGY TRANSFER (meV)

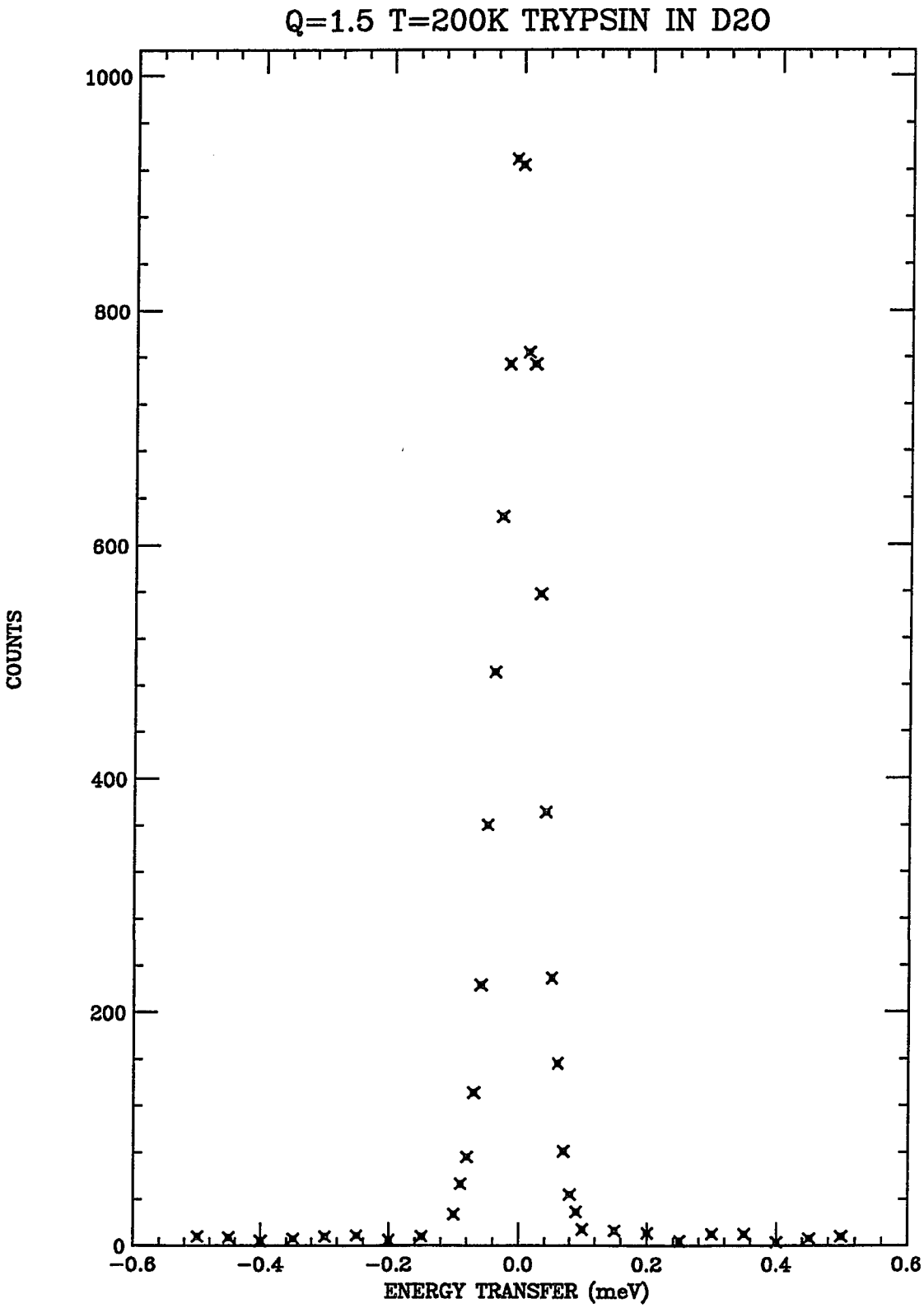
Q=1.5 T=200K TRYPSIN IN D2O
COUNTS
1000
800
600
400
200
0
−0.6
−0.4
−0.2
0.0
0.2
0.4
0.6
ENERGY TRANSFER (meV)

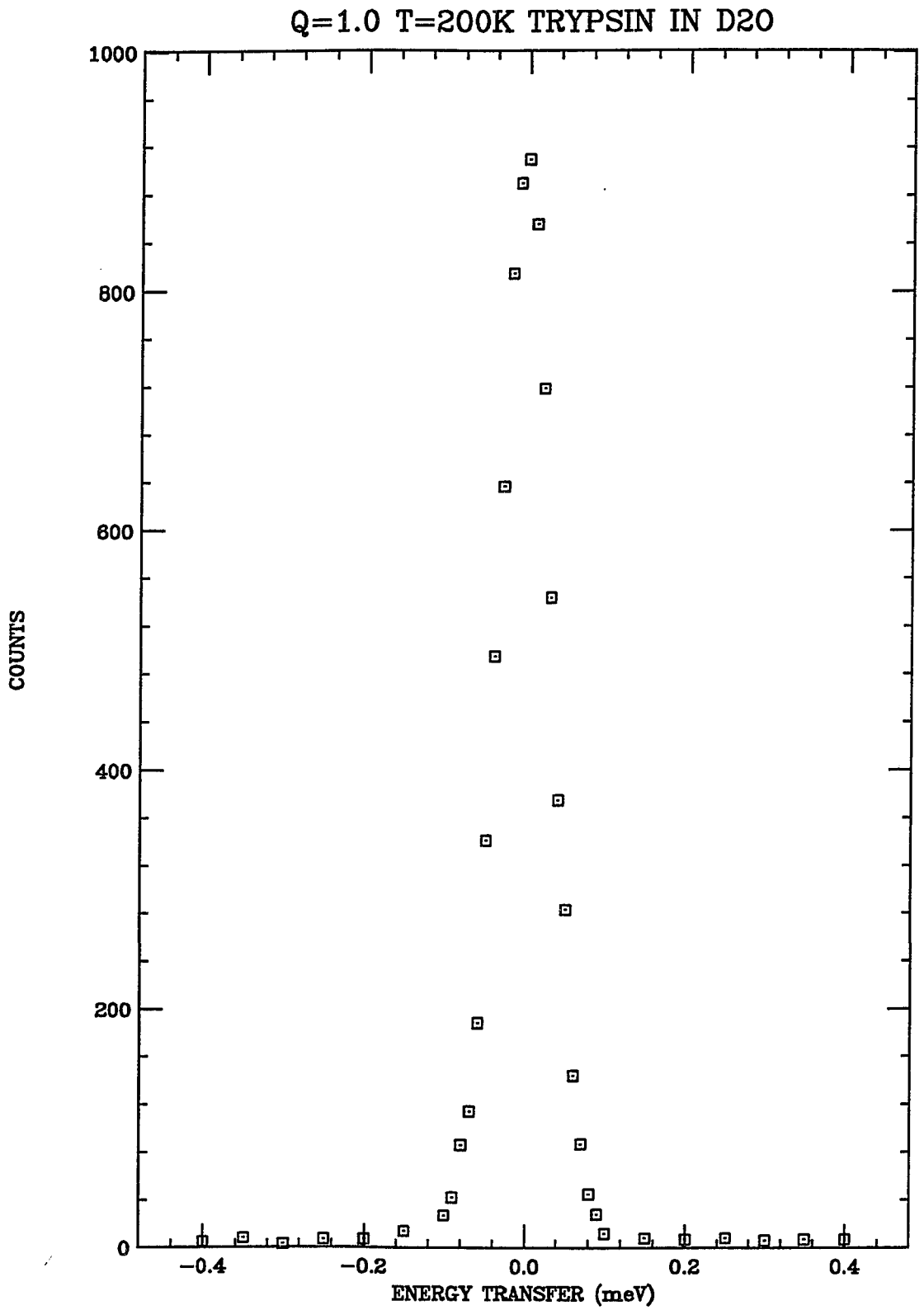
Q=1.0 T=200K TRYPSIN IN D20
1000
800
600
400
200
0
COUNTS
−0.4
−0.2
0.0
0.2
0.4
ENERGY TRANSFER (meV)

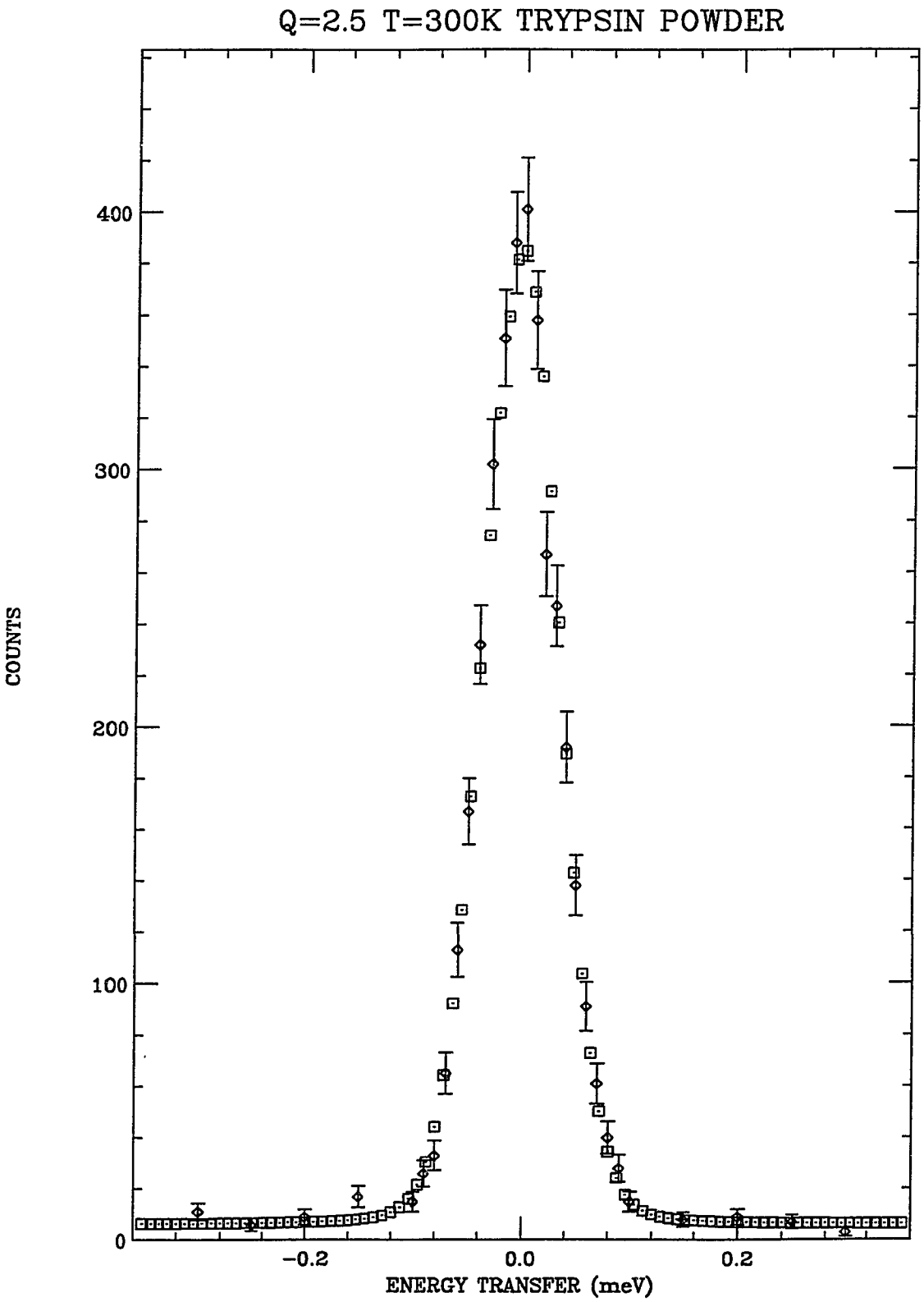
Q=2.5 T=300K TRYPSIN POWDER
COUNTS
400
300
200
100
0
-0.2
0.0
0.2
ENERGY TRANSFER (meV)

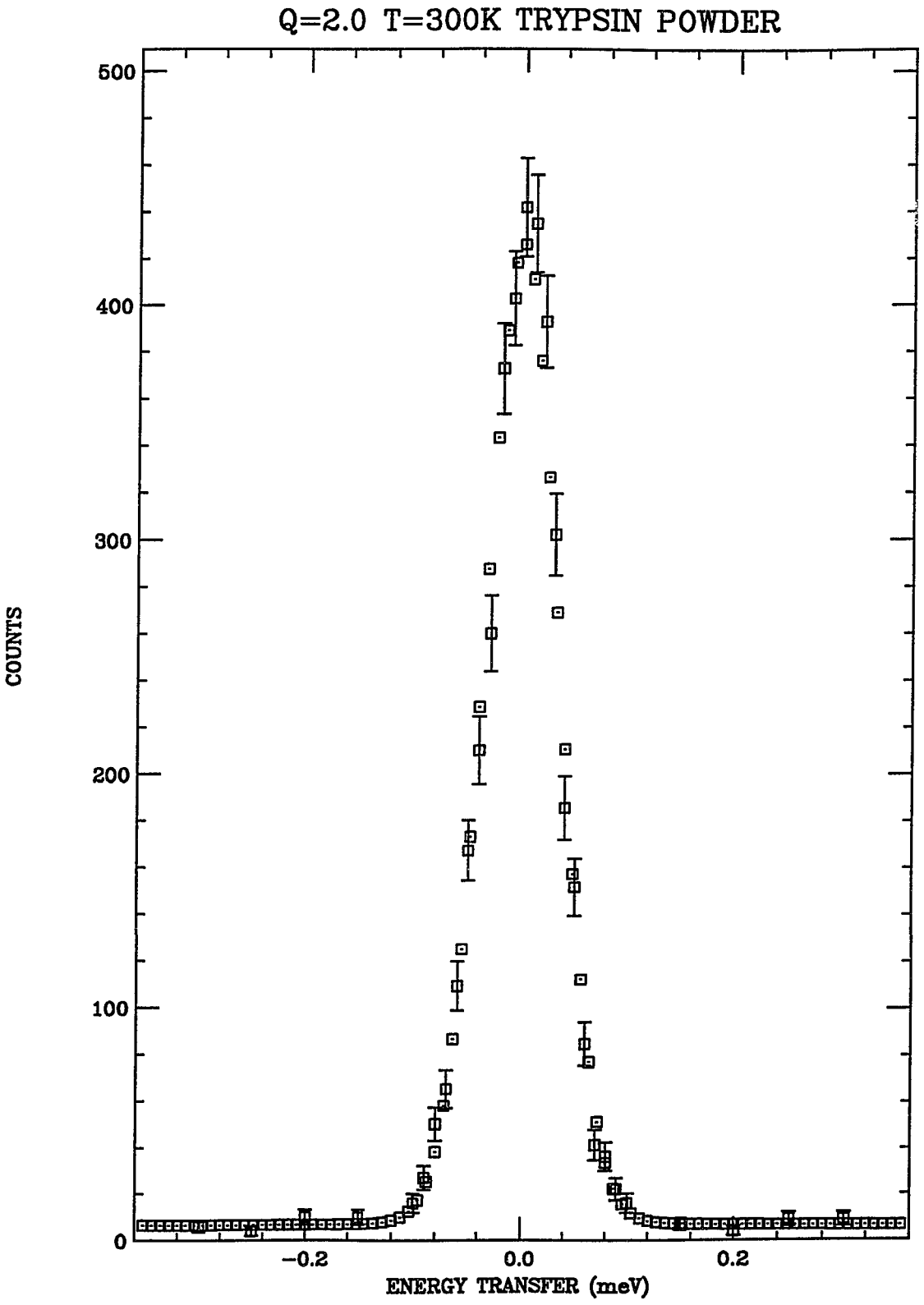
Q=2.0 T=300K TRYPSIN POWDER
500
400
300
200
100
0
COUNTS
−0.2
0.0
0.2
ENERGY TRANSFER (meV)

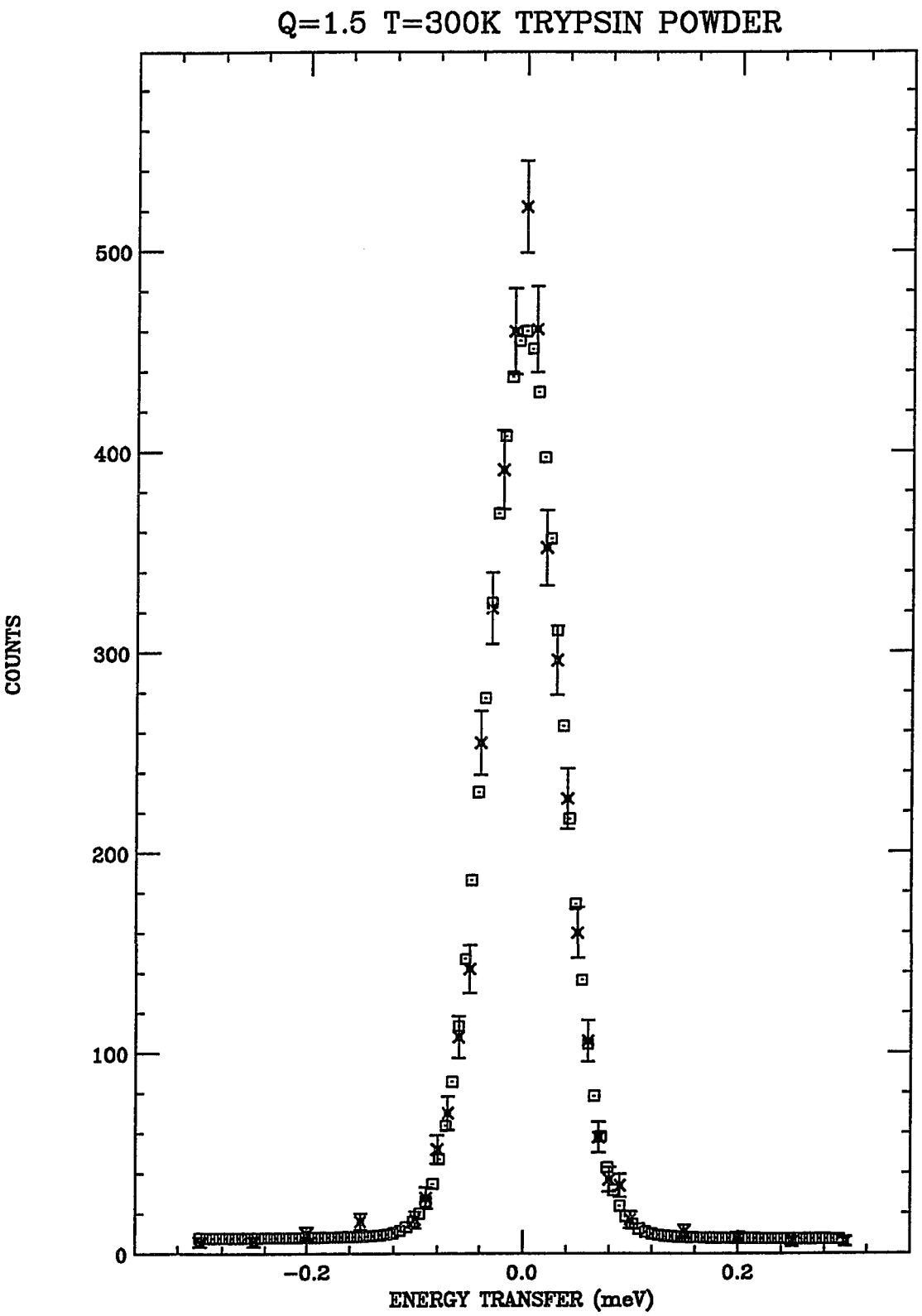
Q=1.5 T=300K TRYPSIN POWDER
COUNTS
500
400
300
200
100
0
-0.2
0.0
0.2
ENERGY TRANSFER (meV)

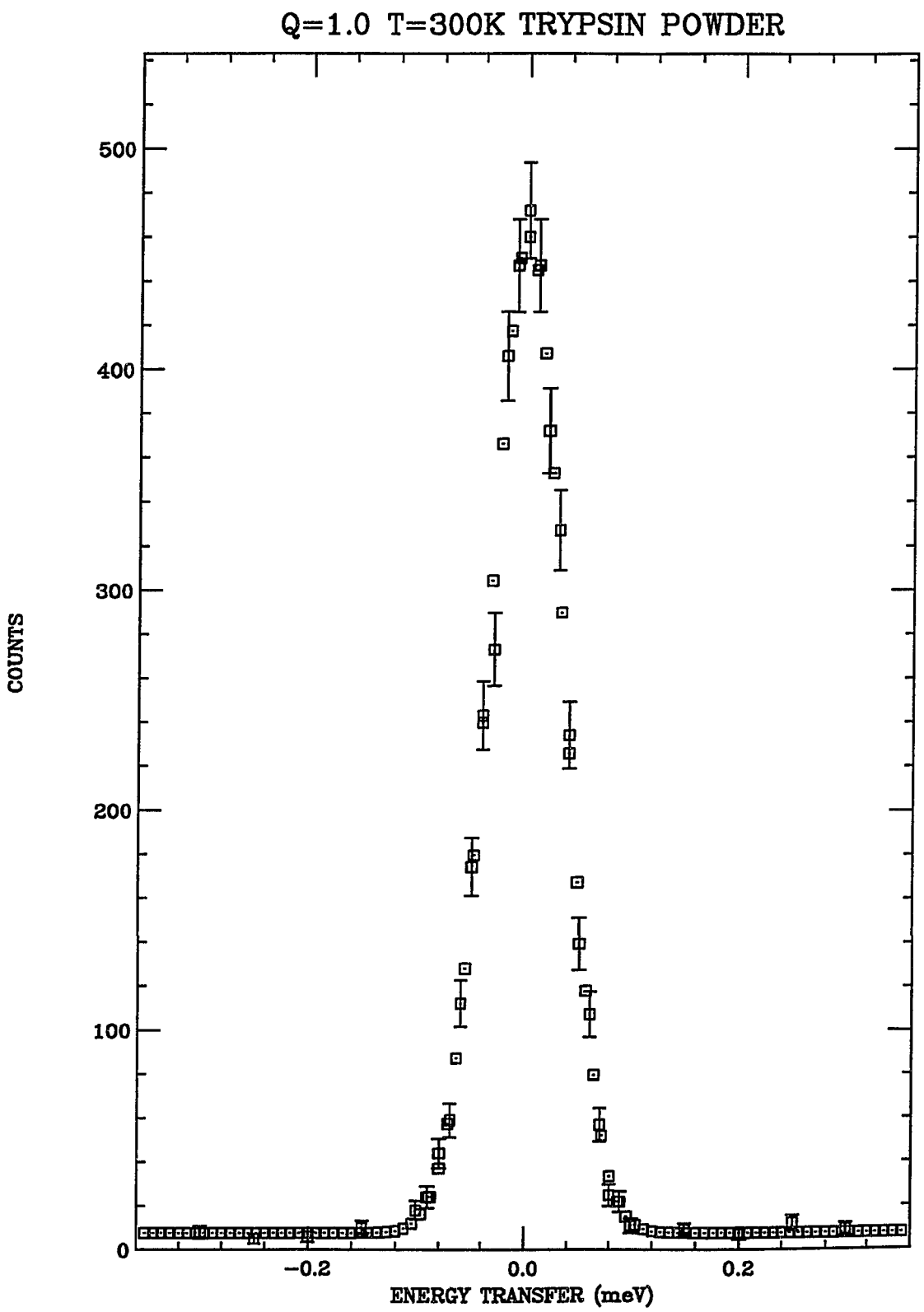
Q=1.0 T=300K TRYPSIN POWDER
COUNTS
500
400
300
200
100
0
-0.2
0.0
0.2
ENERGY TRANSFER (meV)

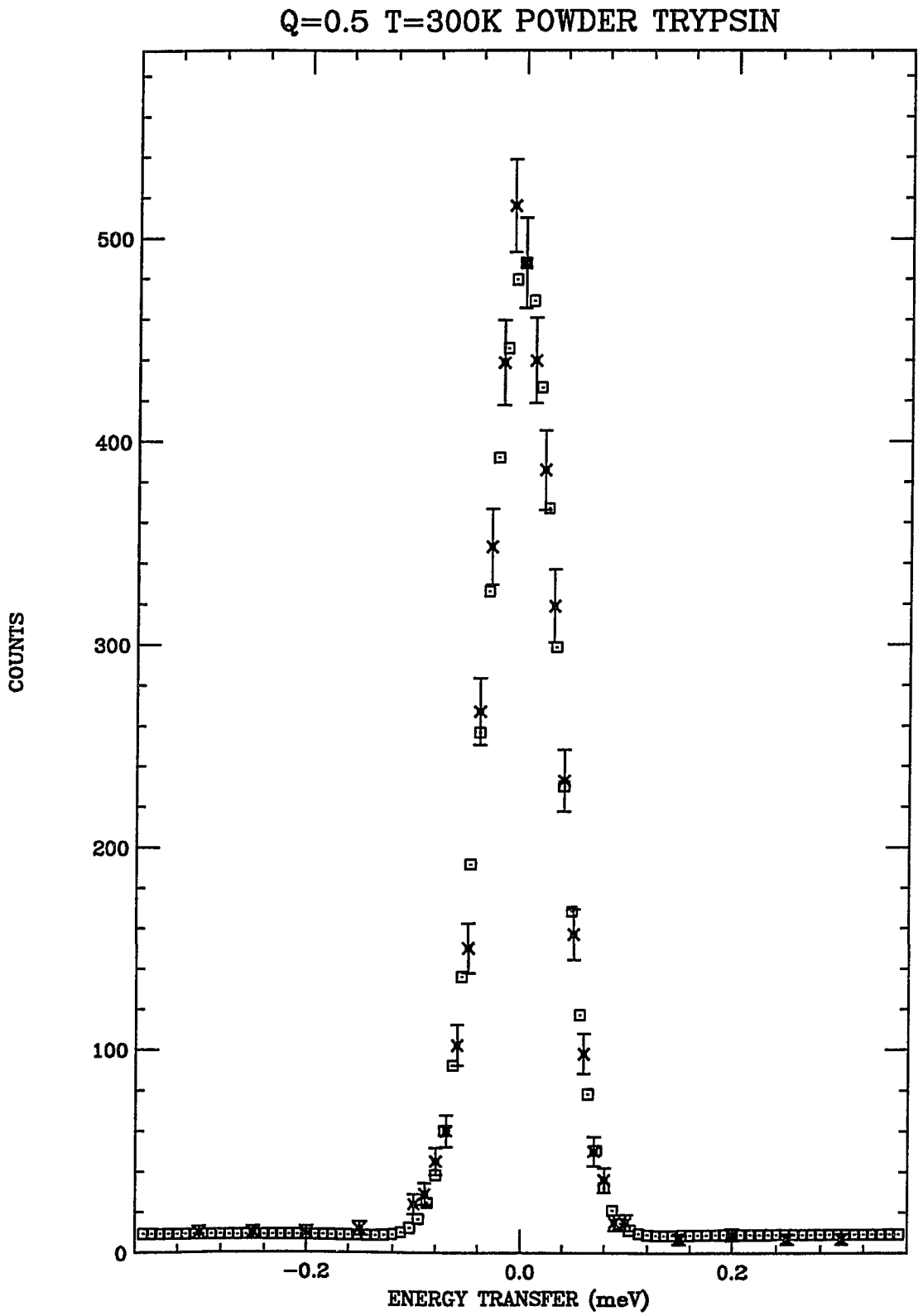
Q=0.5 T=300K POWDER TRYPSIN
COUNTS
500
400
300
200
100
0
-0.2
0.0
0.2
ENERGY TRANSFER (meV)